CALIFORNIA STATE UNIVERSITY, NORTHRIDGE

POST-FIRE DEBRIS FLOW EROSION IN THE SAN GABRIEL MOUNTAINS, CALIFORNIA: EVIDENCE FROM THE STATION FIRE, 2009

A thesis submitted in partial fulfillment of the requirements
For the degree of Master of Science
in Geology

By

Martha M. Ahlstrom

August, 2013

The thesis of Martha M. Ahlstrom is approved:

_____	_____
Dr. Matthew d'Alessio	Date
_____	_____
Dr. Julie Laity	Date
_____	_____
Dr. Richard Heermance, Chair	Date

California State University, Northridge

Acknowledgments

I most heartily thank Dr. Richard Heermance for his exceptional guidance, advice, patience, knowledge, support, and willingness in allowing me to conduct a study on debris flows. My other committee members, Dr. Julie Laity and Dr. Matthew d'Alessio, made heroic efforts in editing my thesis. I appreciate all their efforts to ensure the scientific integrity of this project.

I also thank all the professors in the CSUN Geological Sciences Department for their support. I especially thank Dr. Vicki Pedone for her guidance and encouragement. Mrs. Marilyn Hanna and the Geological Sciences Scholarship Committee funded this thesis project. I am grateful for their support, grants, and scholarships.

This project would have not been completed in such a timely manner without the awesome field assistants who trekked all over the San Gabriel Mountains to help conduct the field work. My field assistants included CSUN undergraduate geology students, CSUN graduate students, Morning Star Christian Academy students, LA Valley College students, and family members. I value all their time and efforts.

I thank all my family members for their patience, graciousness, and support while I completed this project. I especially thank my husband, Eric Ahlstrom, for his continued encouragement and love. For her expert help in creating the figures and illustrations, I am grateful to my daughter, Miki Ahlstrom.

For the acquisition of the NAIP imagery for this project, I robustly thank Dave Annis from the U.S. Forest Service. I also thank Warren Roberts, from the Claremont Colleges Consortium, who served as the GIS consultant to this project.

Lastly, I thank God who gave me the faith, fortitude, and perseverance to complete this project.

Table of Contents

List of Tables

List of Figures

List of Equations

ABSTRACT

POST-FIRE DEBRIS FLOW EROSION

IN THE SAN GABRIEL MOUNTAINS, CALIFORNIA:

EVIDENCE FROM THE STATION FIRE, 2009

By

Martha M. Ahlstrom

Master of Science in Geology

Debris flows are a source of substantial erosion in mountainous areas. Consequently, their occurrence, spatial density, and characteristics provide essential data for understanding erosion rates and volumes. The 2009 Station Fire in the San Gabriel Mountains burned an extensive area (650 square km), and thus destabilized the slopes setting them up for subsequent debris flows. GIS mapping of 58 post-fire debris flows, within the burn area the first year after the fire, allowed the quantification of debris flow density within the burn area. Most debris flows were initiated from burned, previously undisturbed, upper channel hill slopes averaging 28°. The spatial density was one flow per every two square kilometers. Nine flows were chosen for field investigation and debris volume determination. Debris flow volumes from the field measured flows were correlated with drainage basin area above each flow to reveal a positive linear correlation of 0.053. The correlation coefficient was then used to calculate total material from each drainage area affected. Total flow material deposited was 717,300 ± 179,310 cubic meters and covered 6% of the total burn area. The volume of deposition can be quantitatively determined based on the regression equation of V = 0.053A, (V = volume

in cubic meters, A = area in square meters). Based on a fire recurrence interval of every 30 years in the San Gabriel Mountains, post-fire debris flows account for 0.13 ± 0.02 mm/yr of erosion within the burn area. This erosion rate accounts for ~10% of the total erosion rate of ~1 mm/yr determined for this area in the San Gabriel Mountains, despite flows covering only 6% of the area. These data provide an empirical dataset for future debris flow hazard analysis, as well as providing a quantitative assessment of post-fire erosion rates in the San Gabriel Mountains.

Chapter 1: Introduction

Post-Fire Debris Flows

Recently burned sections of mountainous areas typically yield much greater amounts of soil and debris than those not burned (Cannon et al., 2001). Burnt landscapes are especially susceptible to debris flows because fires radically alter physical soil properties, causing loss or reduction of soil structure, loss of organic material, reduced porosity, and increased pH. Most of the changes to the soil are caused by an alteration in the soil chemistry due to high temperatures and oxidation, which results in complex interactions among geomorphic processes, climate, vegetation, and landforms (Bruhjell and Tegart, 2006). A hydrophobic layer forms in the soil when naturally occurring waxy organic compounds are vaporized by the fire forming a discrete layer, which impedes water infiltration, and combined with the destruction of the vegetative layer increases runoff resulting in an increase in erosion. In addition, the ash left behind from fires forms an impermeable layer that increases surface runoff and the probability of debris flows (Cannon et al., 2001; Moody et al., 2005; Gabet and Sternberg, 2008). These scorched areas are highly unstable and the subsequent debris flows cause considerable erosion (Cannon et al., 2010). In fact, the first year after a fire, erosion rates are estimated to be approximately 15 to 35 times greater than normal, and do not return to normal until at least 5 years later (Tan, 1998; Warrick et al., 2012).

Debris flows are concentrated mixtures of various sediment and water, which flow downslope by gravitational forces with highly unsteady, surging flow behaviors. With a much higher viscosity than regular flood waters, debris flows maintain a relatively coherent mass as they progress downslope. The front edge of a debris flow, deemed the

head, contains boulder-sized clasts and is followed by a highly viscous mass that transitions into a sandy, muddy water flow as it travels down a channel (Iverson, 1997). Debris flows comprise a major natural hazard. They often occur with little warning, cause significant damage to infrastructures, strip the land of vegetation, deposit massive amounts of debris, and endanger lives (Major and Iverson, 1999; Cannon and DeGraff, 2009; McCoy et al., 2010). See Figure 1 for a schematic of a post-fire debris flow.

Debris flows cause significant hillslope erosion. Kean et al. (2011) monitored twenty-four debris flows in 2010 in the Station Fire burn area and determined that all these flows were generated by the progressive entrainment of sediment from hillslope rilling and channel erosion. Debris flow initiation was correlated with short duration, high intensity rainfall, and lagged behind the rainfall by 5 minutes. They observed through post-event erosion and slope stability modeling that debris flows initiated mostly by processes related to surface water run-off, rather than shallow landslides. In the first year after a fire, the onset of post-fire debris flows is tied to high intensity rainfall producing overland flow.

Warrick et al. (2012) stated that wildfires and subsequent intense rainfall caused erosion rates to increase over long-term average rates and are an important forcing role in large sediment yields from debris flow areas. Many debris flows in burn areas occur in response to small storms, but they become catastrophic when a severe burn is followed by relentless rains (Figure 2). The potent force of debris flows (rapidly moving water, soil, and rock) destroys buildings, roadways, culverts, and bridges and can cause injury or death (Scott and Williams, 1978; McPhee, 1989; Slosson and Shuriman, 1992; Cannon, 2010; Warrick et al., 2012). Understanding and predicting erosion rates in the San

Gabriel Mountains is important because erosion leads to sediment transport, rock exposure, soil destruction, and sediment deposition (Portenga and Bierman, 2011).

Processes of Sediment Production

In the San Gabriel Mountains interactions between erosion, climate, and fires control the major sediment production. According to Lavé and Burbank (2004), shallow landsliding on soil slopes accounts for almost half of the hillslope erosion; bedrock landsliding is $\leq 1/3$ of the total erosion; hillslope sediment stored in upper channels are moved only during large, infrequent storms; and, in slower denuding catchments, shallow landsliding or wet and dry ravel cause the major erosion. They conclude that fires followed by intense storms typically generate the largest sediment fluxes.

Schematic of a Post-Fire Debris Flow

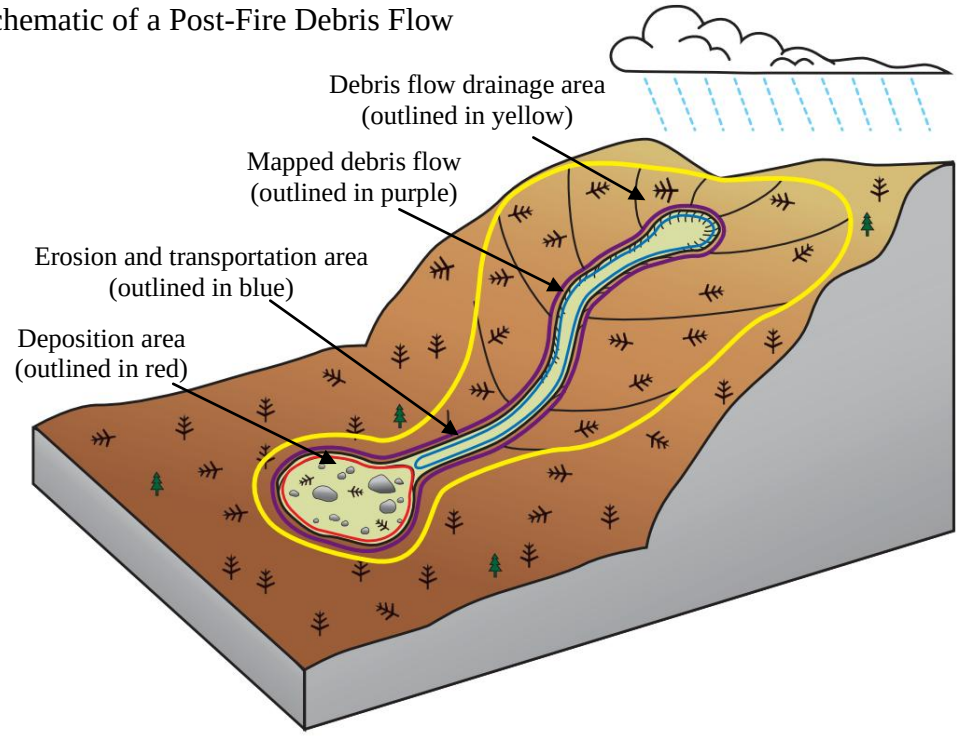

Figure 1: Schematic diagram of a typical post-fire debris flow in the San Gabriel Mountains

Effects of Wildfire on Sediment Deposits from a Steep, Chaparral Landscape

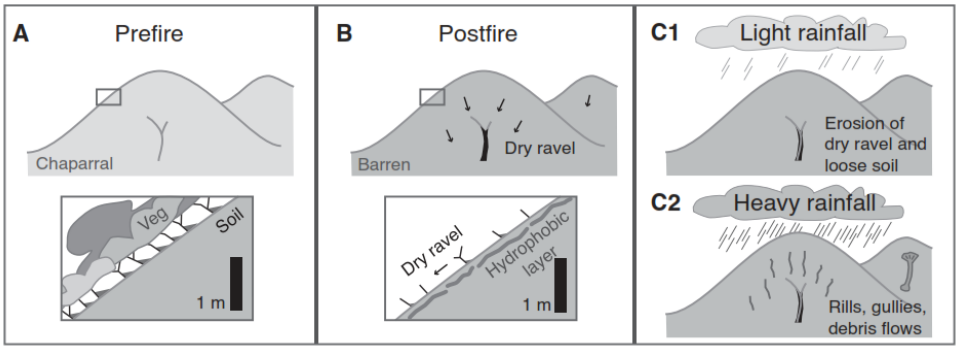

Figure 2. Effects on wildfire on sediment deposits from a steep, chaparral landscape:

A. Before a fire, the chaparral vegetation and organic debris retain sediment.
B. During and after a fire, the combustion of vegetation and organic debris above the ground reduces surface roughness and releases dry ravel, which accumulates in colluvial areas, hillslopes, and steam channels. The high temperature of chaparral fire causes a hydrophobic layer beneath the soil.
C. Sediment erosion and transport processes during post-fire rainfall are dependent on rainfall intensity.
   1. Light rainfall will result in the erosion of loose soil and dry ravel talus.
   2. Medium to heavy rainfall will generate overland flows that can cut rills and gullies into the soil and generate debris flows.
   (Adapted from Warrick et al., 2012)

The Station Fire of 2009

The Station Fire in the Angeles National Forest commenced on August 26, 2009 and was not contained until October 16, 2009 (Figure 3). It burned 160,560 acres (650 km^2), making it one of the largest in modern California history and the largest in Los Angeles County history (Los Angeles County Fire Department, 2009) (Figures 3 and 4). Afterwards, the intense winter rains caused debris flows to occur predominately on the steep debris flow drainage areas, which had not had recent debris flows. Ten powerful rainstorms which all generated debris flows occurred from November 2009 to February 2010 (Figure 5). The rainfall for winter of 2009-2010 was higher than the average rainfall due to an El Niño event (which is caused by a prolonged difference in the Pacific Ocean sea surface temperatures, warming or cooling of at least 0.5°C, compared with the average value). These rainstorms ranged between 45 minutes to 56 hours in duration and had rainfall totals per storm between 1.3 and 17.45 cm (Cannon et al., 2011). In several canyons of La Canãda-Flintridge and Glendale, debris flows over 8 m in depth rapidly developed and destroyed roads and property, including several houses and cars (L.A. Times, 02/06/2010).

The effect of post-fire debris flows on the overall erosion rates in the San Gabriel Mountains is the focus of this study. Consequently, the purpose of this project is to characterize the post Station Fire debris flows, calculate the amount of debris entrained within these flows, and calculate the contribution of these types of flows to the overall erosion rates. The hypothesis tested is thus that post-fire debris flows in the San Gabriel Mountains, although infrequent, greatly increase the erosion rates and are a significant contributor to the overall erosion rates.

Station Fire (2009)

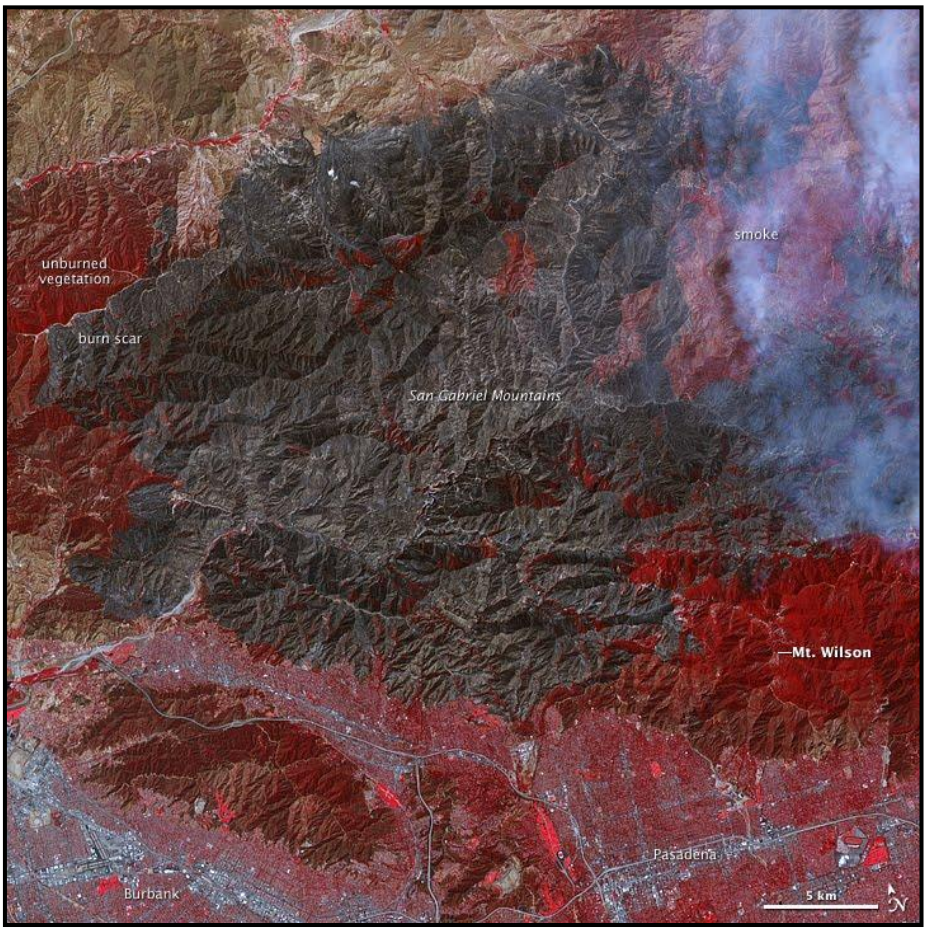

Figure 3. Station Fire (2009) from NASA (2009)

Location Map of San Gabriel Mountains

Figure 4. Reference location map of San Gabriel Mountains with the Station Fire burn perimeter. The shaded relief imagery was developed by ESRI using GTOPO30, Shuttle Radar Topography Mission (SRTM), and National Elevation Data (NED) data from the USGS. The burn perimeter shapefile is courtesy of the U.S. Forestry Department.

Rainfall History for Winter 2009-2010

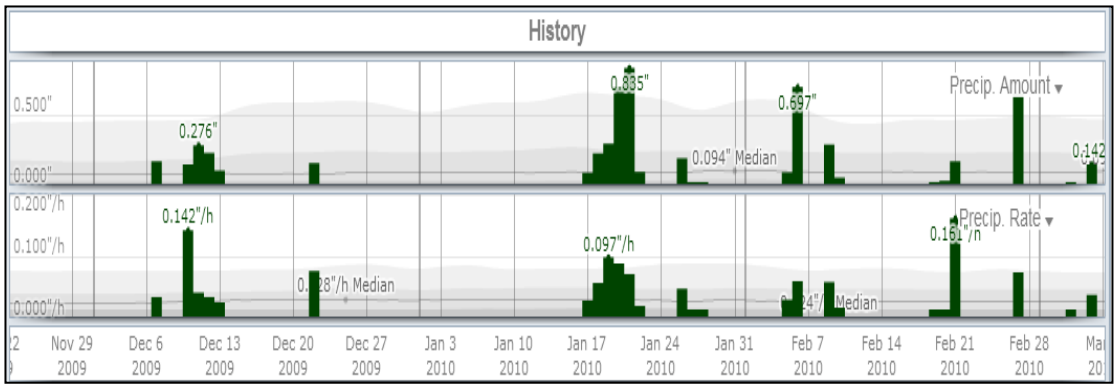

Figure 5. Rainfall history from November 2009 – February 2010 for San Gabriel Mountains totaled over 760 mm measured at San Gabriel Mountains weather station (see location on Figure 9) (downloaded from weatherspark.com)

Chapter 2: Wildfires in the San Gabriel Mountains

Wild fires greatly enhance the generation of debris flows in the San Gabriel Mountains. Numerous fires and destructive post-fire debris flows have occurred in the last hundred years including 1914, 1935, 1969, 1978, and 2003, and are recognized in the literature (Eaton, 1936; LACFCD, 1959; McFee, 1989; Cannon, 2010) (Figure 6). Southern California, which has a Mediterranean climate with warm, dry summers and cool, wet winters, experiences frequent wildfires that occur immediately preceding the winter rainy season. Occasionally, there are fires in the spring. On average, each slope in the San Gabriel Mountains is burned every 30-50 years (Hellmers, 1962). These fires often coincide with the dry intense Santa Ana winds, which occur when high pressure systems develop over the Great Basin. Air flows from the desert to the sea, contrary to the prevailing Westerly flow. Humidity levels commonly drop below 10% and the winds are topographically accelerated. Santa Ana conditions intensify fires, which are difficult to control until the weather conditions change or all fuels are consumed. This type of fire, called a ground fire, has intense blazes that strip the vegetation and organic matter down to bare rock (Ainsworth and Doss, 1995). Vegetation type also contributes to wild fire susceptibility. Most of the vegetation in the San Gabriel Mountains is chaparral, drought-resistant plants, which are small shrubs with hard and small leaves, are non-deciduous and highly flammable. Chaparral thrives on the long, dry, hot summers and receives most of its annual rainfall, between 254 - 813 mm/yr, in the winter rains (Radtke, 1983). The San Gabriel Mountains rise rapidly from the foothills with steep-sided slopes ranging from 35% up to 65-70% (Figure 7). The majority of a burned area is on the steep, brush covered slopes drained by steep channels encouraging debris flows. Sediment production

increases tremendously after the fires, as the fires help to destabilize the soil, sediments, and rocks. The subsequent post-fire debris flows then increase the erosion rates (Cannon and De Graff, 2009). Furthermore, the increase of anthropogenic fires has accelerated the rates of erosion within small, steep catchments next to populated areas, such as in Los Angeles County (Lavé and Burbank, 2004).

Documented Fires in the San Gabriel Mountains

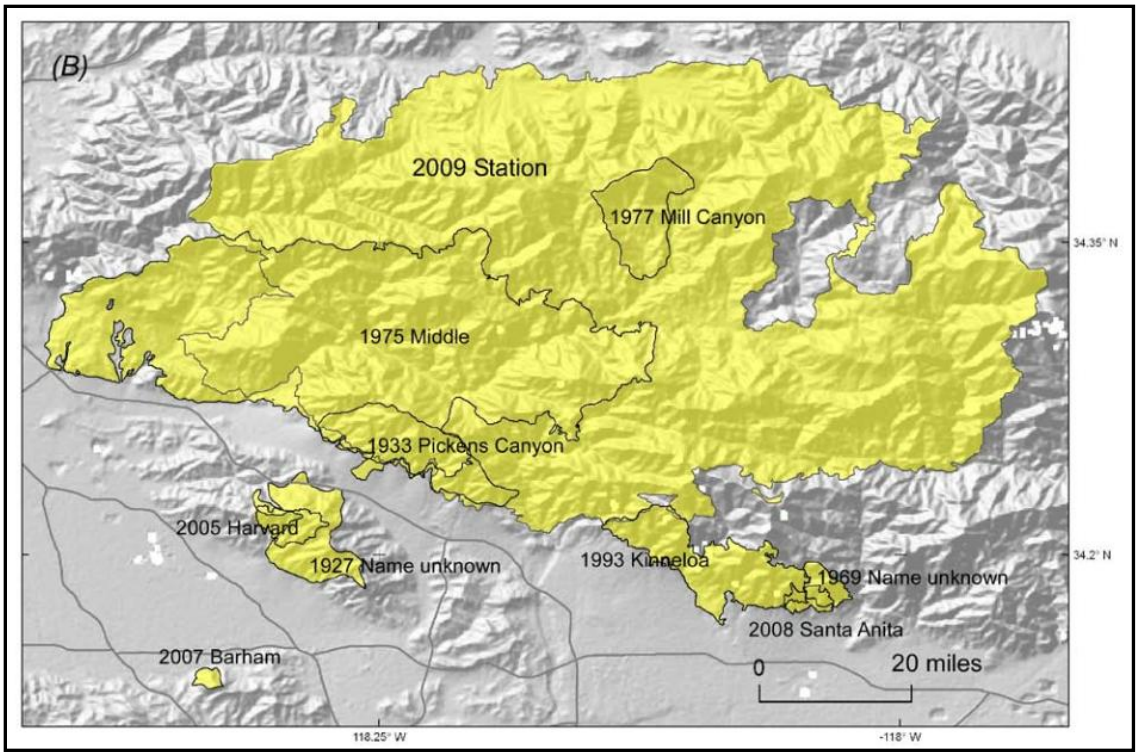

Figure 6. Documented fires in the San Gabriel Mountains in the last century, burned areas in yellow with post-fire debris flows (Cannon et al., 2010)

View of the San Gabriel Mountains to the North

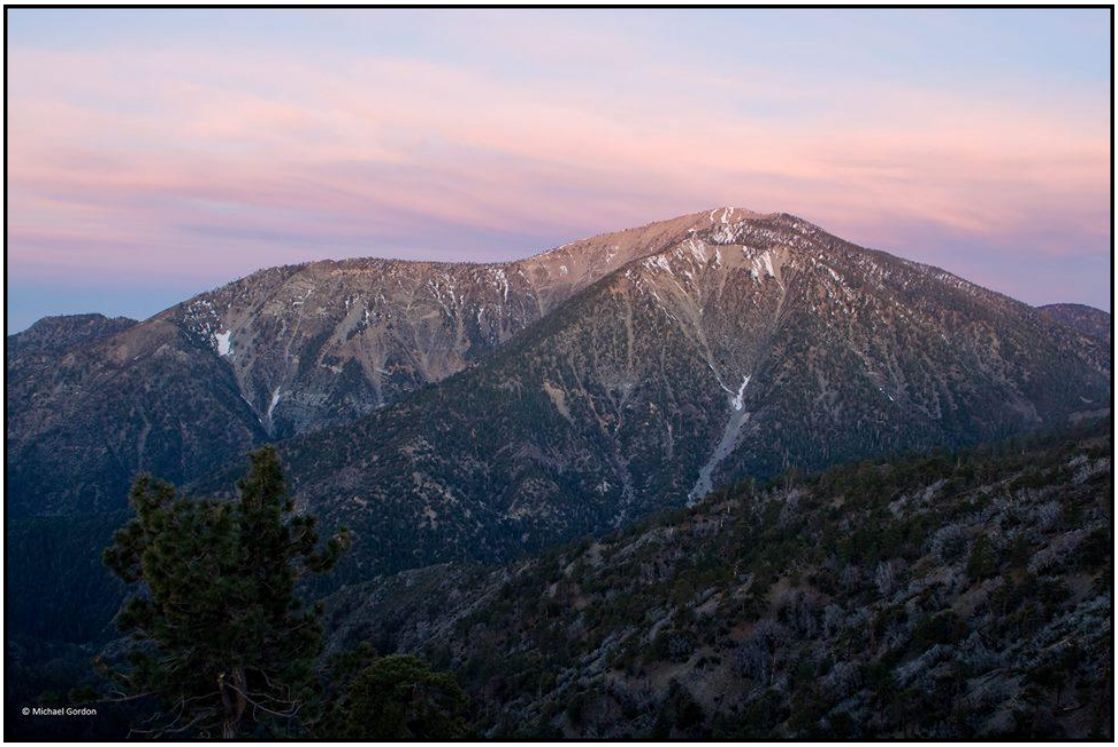

Figure 7. View of the steep-sided slopes of the San Gabriel Mountains to the north (Michael Gordon, 2013)

Chapter 3: Historical Erosion in the San Gabriel Mountains

Since 1928, debris flow basins were built in Los Angeles County to catch the flows and stop their encroachment on the urbanized southern front of the San Gabriel Mountains. These basins fill with sediment, and must be periodically cleaned out in order to retain their effectiveness. Lavé and Burbank (2004) examined 75 of these debris basins and estimated sediment deposition for the period 1928-1973, based upon the documented Los Angeles County Department of Public Works (LACDPW) removal of the sediment. These volumetric data show an increase in sediment flux during this period that is believed to have resulted from an increase in fire frequency over the past century. These debris basins show increased sediment delivery by an average of $\geq 60\%$ and some basins show increases up to 400% since first being built, due to the increase in fires (natural and anthropogenic) and subsequent debris flows (Lavé and Burbank, 2004).

Cannon et al. (2008) researched several post-fire debris flow areas in the southwestern United States, including those generated after the Old and Grand Prix fires of 2003 in the San Gabriel and San Bernardino Mountains. Although this study focused primarily on the rainfall threshold conditions necessary to generate debris flows, it showed a definite link between increased wildfires and increased debris flow occurrences and the need to clean out the debris flow basins more frequently than before 2003.

.

Chapter 4: Geologic Setting

The San Gabriel Mountains (SGM) are part of the Transverse Ranges Province of southern California and are a fault-bounded block of crystalline rocks north of the Los Angeles Basin. To the north, the mountains descend to the Mojave Desert Province and to the west into the Sierra Pelona and the Soledad Basin (Figure 8). To the east, the mountains rise in elevation to a maximum of 3068 m. The San Andreas Fault system forms the northern boundary of this range and is indirectly responsible for the growth of the Transverse Ranges due to the role of transpression in the development of this orogen, including the San Gabriel Mountains. The Cucamonga-Sierra Madre fault complex is on the south and southwest portion of the range (Matti et al., 1992; Lavé and Burbank, 2004).

The basement rocks of the SGM are characterized by Precambrian and upper Mesozoic metamorphic and plutonic rocks. Upper Cretaceous age granite plutons intruded into Upper Triassic granodiorites and Precambrian gneiss-amphibolite-granite and anorthosite-syenite-gabbro complexes. Metamorphosed sedimentary rocks and plutonic rocks in the southeastern SGM are interrupted by a belt of mylonite (Matti et al., 1992).

The SGM debris flow channels consist of igneous and metamorphic rocks, including schist, gneiss, and meta-sedimentary rocks. Clastic sedimentary rocks are lacking in the SGM watersheds. Rocks are commonly jointed and fractured in the watershed areas, are highly weathered, and susceptible to frequent landslides and debris flows. Soils are rocky, sandy loams, have a high organic content, and are generally less than one meter thick (Lustig, 1965).

Steep-sided deep canyons are characteristic of the SGM. Some slopes are as steep as 65-70 %. This is attributed to the fact that the mountains are rising as much as 5 mm/yr (San Gabriel Mountains and Watershed Special Resource Study and Environmental Assessment, 2012). Elevations range from 1219 meters at Red Mountain (one of the lowest peaks) to 3068 meters at Mount Baldy (the highest peak). As the SGM have lofty elevations and the drainage systems of the watersheds have substantially lower elevations, the relief values are high (San Gabriel Mountains and Watershed Special Resource Study and Environmental Assessment, 2012). The canyon sides are covered with unstable hill-slope rock debris which is constantly being eroded by slope failures, runoff, and debris flows. After a fire, there is a loss of mechanical support provided by existing organic material. This loss facilitates further formation of dry ravel (gravity inducted material) on the steep slopes and in the debris flow channels. This fire-induced dry ravel increases the sediment volume in a debris flow (Matti et al., 1992; Cannon et al., 2010).

Geologic Location of the San Gabriel Mountains

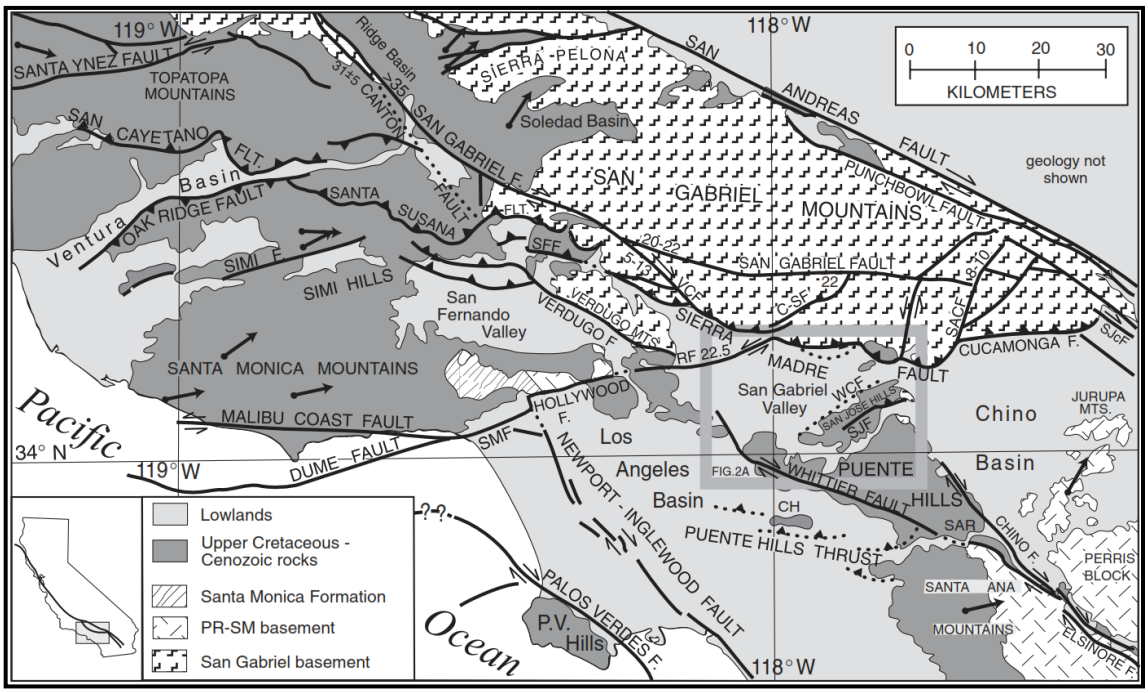

Figure 8. Geologic location map of the San Gabriel Mountains (Yeats, 2004)

Chapter 5: Study Area in the San Gabriel Mountains

The study area is located in the southwestern San Gabriel Mountains within the Sunland, Burbank, Condor Peak, and Pasadena USGS Quadrangles and within the Station Fire burn perimeter, north of Sunland and La Canãda-Flintridge. This study area was chosen because of its close proximity to roads and because it is a highly populated area. It is approximately 192 km^2, which is 30% of the entire area affected by the Station Fire. The study area is an irregular shape and is roughly 11.0 x 17.3 km (Figure 9). The terrain of this area of the San Gabriel Mountains is dominated by steep canyons with jagged sides whose debris flow channels debouch into populated foothill areas. The debris flow channels studied include Gold Canyon, Ybarra Canyon, Pickens Canyon, Dark Canyon, Stone Canyon, Delta Canyon, a small unnamed canyon next to Delta Canyon, Vogel Canyon, and Arroyo Seco Canyon (Table 1). They are accessed by roads (Highway 2 and Big Tujunga Canyon Road), as well as numerous hiking trails.

Due to the large size of the Station Fire area only the southwestern quadrant was mapped for post Station Fire debris flows. The study assumption is that the remaining unmapped area is similar in the frequency and size of debris flows, the degree and nature of erosion, and that results from the study area can be extrapolated to other burn areas. This is reasonable because the basic geologic materials, slope angles, vegetation cover, and amount and intensity of rain vary little over the area of the Station Fire, located in the southern portion of the San Gabriel Mountains (San Gabriel Mountains and Watershed Special Resource Study and Environmental Assessment, 2012).

Study Area

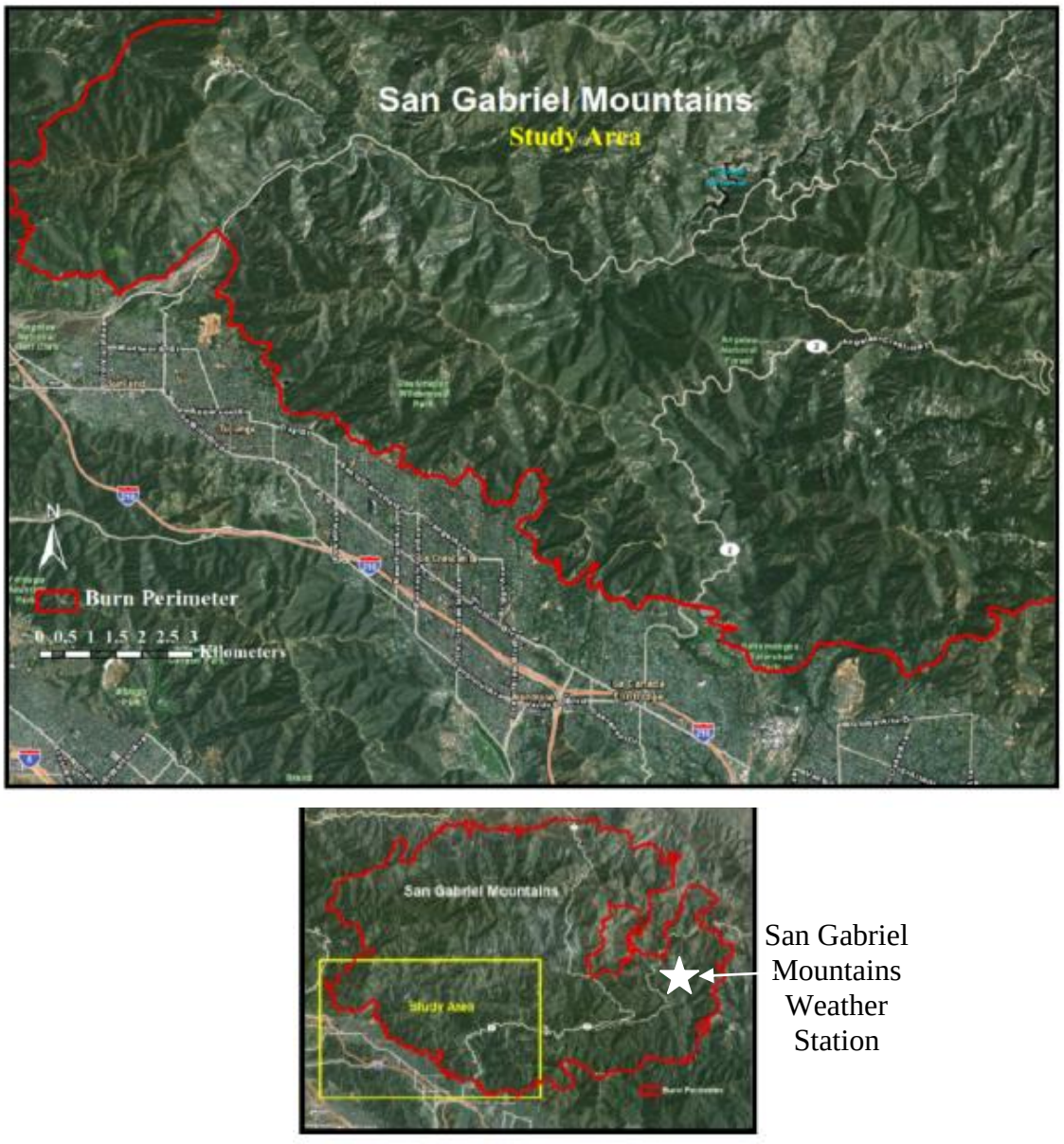

Figure 9. The study area is in the southwestern San Gabriel Mountains within the Station Fire burn perimeter and covers approximately 192 km^2. White star shows the San Gabriel Mountains weather station location. Imagery is from the United States Department of Agriculture (USDA) National Agriculture Imagery Program (NAIP) imagery and enhanced versions of United States Geological Survey (USGS) Digital Ortho Quarter Quad (DOQQ) imagery.

Debris Flow ID with GPS Points

Debris Flow ID	GPS Location Point
2 (Gold Canyon)	34°18'04.92"N 118°16'15.91"W
16 (Ybarra Canyon)	34°17'59.30"N 118°14'45.54"W
22 (Pickens Canyon)	34°13'22.32"N 118°13'41.96"W
43 (Dark Canyon)	34°15'35.94"N 118°11'48.83"W
48 (small canyon tributary east of Delta Canyon)	34°17'46.31"N 118°14'41.74"W
49 (Delta Canyon)	34°18'07.40"N 118°15'38.41"W
50 (Vogel Canyon)	34°17'24.14"N 118°13'30.92"W
52 (Stone Canyon)	34°17'19.08"N 118°13'59.75"W
56 (Arroyo Seco Canyon)	34°12'12.95"N 118°09'58.51"W

Table 1. Debris flow ID and corresponding canyon names with GPS location points for each field measured flow. GPS points are located near the toe (or basin) of each debris flow for easy accessibility from a road or trail.

Chapter 6: Methods

The purpose of this study is to characterize the Station fire debris flows by remote mapping, field mapping, lithological analyses, compare the debris flow drainage areas to the volume of debris flow deposits, and calculate a debris flow erosion rate.

Figure 10 illustrates the overall workflow to accomplish this goal. Step one was to utilize remote imagery to map the pre-fire scarps from earlier debris flows from imagery obtained from July 2009. Step two involved remote-mapping of debris flows that occurred shortly after the Station Fire in late 2009 and early 2010 (based on imagery taken from April to September 2010). Step three involved field mapping of nine selected debris flows to determine the transition areas from erosion to deposition, to measure the volumes of debris flow deposited, to measure the slope where the flows commenced deposition, and to conduct lithological analyses. Step four involved remote mapping of the drainage systems for each debris flow. Step five involved the calculation of debris volume from the measured debris flows. Step six involved a regression analysis of the mapped flows and extrapolation of this regression to all the remotely mapped flows within the study area. In step seven, the final step, the approximate erosion rates due to these types of debris flows were calculated.

Work Flow for Station Fire (2009) Debris Flows.

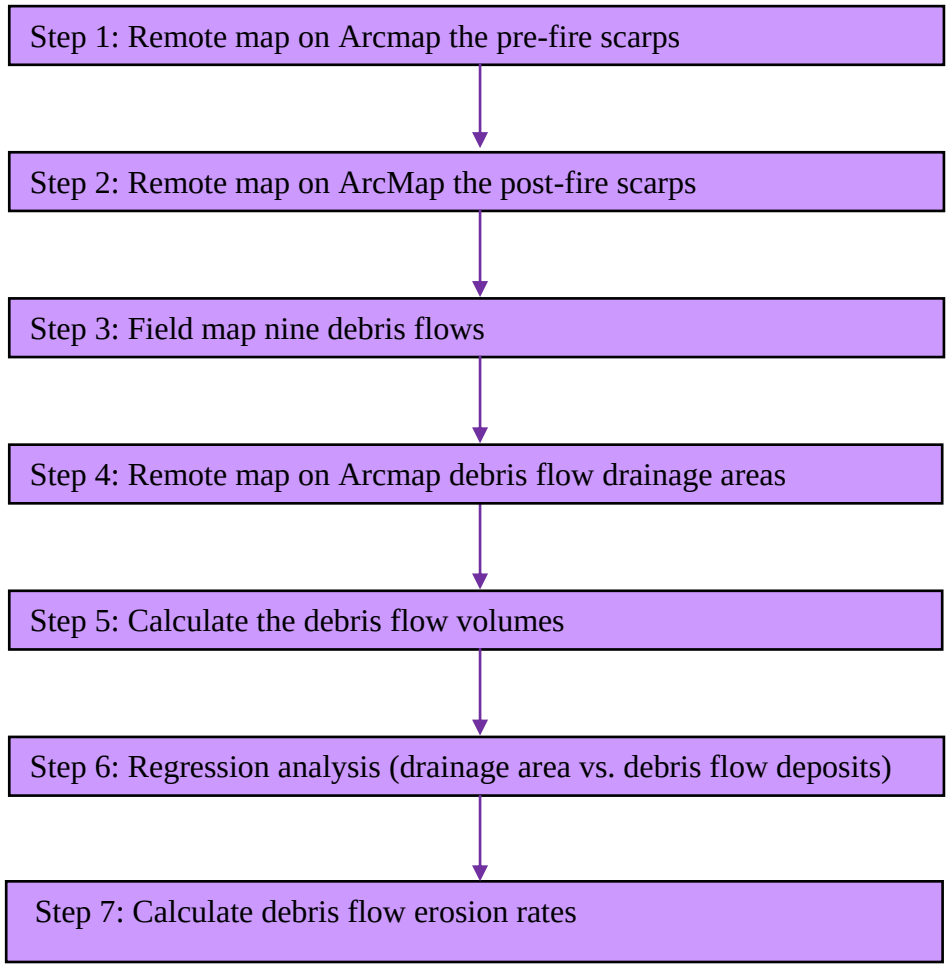

Figure 10. Step by step process for analysis of Station Fire (2009) debris flows

Pre-Fire Remote Imagery Mapping

To assist in the pre-fire mapping, digital elevation models (DEMs) and aerial photography from July 2009 were obtained from The National Map Viewer, a service on the USGS website. Imagery is from the United States Department of Agriculture (USDA), National Agriculture Imagery Program (NAIP), and enhanced versions of United States Geological Survey (USGS) Digital Ortho Quarter Quads (DOQQ), see Table 2 for imagery information. All images were ortho-rectified as Arcmap layers in ArcGIS 10 for the study area in the San Gabriel Mountains. Subsequently, the Station Fire burn area shapefile (obtained from the U.S. Forestry Service), as well as the USGS quadrangle images (obtained from the USGS), were added to Arcmap. The pre-fire debris flow boundaries were then systematically identified and mapped by hand on the Arcmap in the study area (Figure 11). These pre-fire scarps or scars were identified by their distinctive head scarps, residual depositional lobes, and hummocky terrain on the steep slopes in the pre-fire aerial photographs.

Ariel Photography Source Information for Pre-Fire ArcMap

Sources	Resolution	Rectification Accuracy	Rectification method	Spatial Reference
National Agriculture Imagery Program (NAIP), USDA, and USGS	1 meter GSD	± 5 meters of the reference DOQQs	ortho imagery rectified	UTM (Zone 11N) using the NAD 1983

Table 2. Aerial photography source information for pre-fire Arcmap

Ariel Photography Source Information for Post-Fire ArcMap

Source	Sections	Resolution	Rectification Accuracy	Rectification method	Spatial Reference
National Agriculture Imagery Program (NAIP)	Section 1	1 meter GSD	± 5 meters of the reference DOQQs	ortho imagery rectified	UTM (Zone 11N) using the NAD 1983
	Section 2	2 meter GSD	± 10 meters of the reference DOQQs		
	Section 3	1 meter GSD	± 6 meters of the reference DOQQs		
	Section 4	2 meter GSD	± 10 meters of the reference DOQQs		

Table 3. Aerial photography source information for post-fire Arcmap

Pre-Fire Mapping

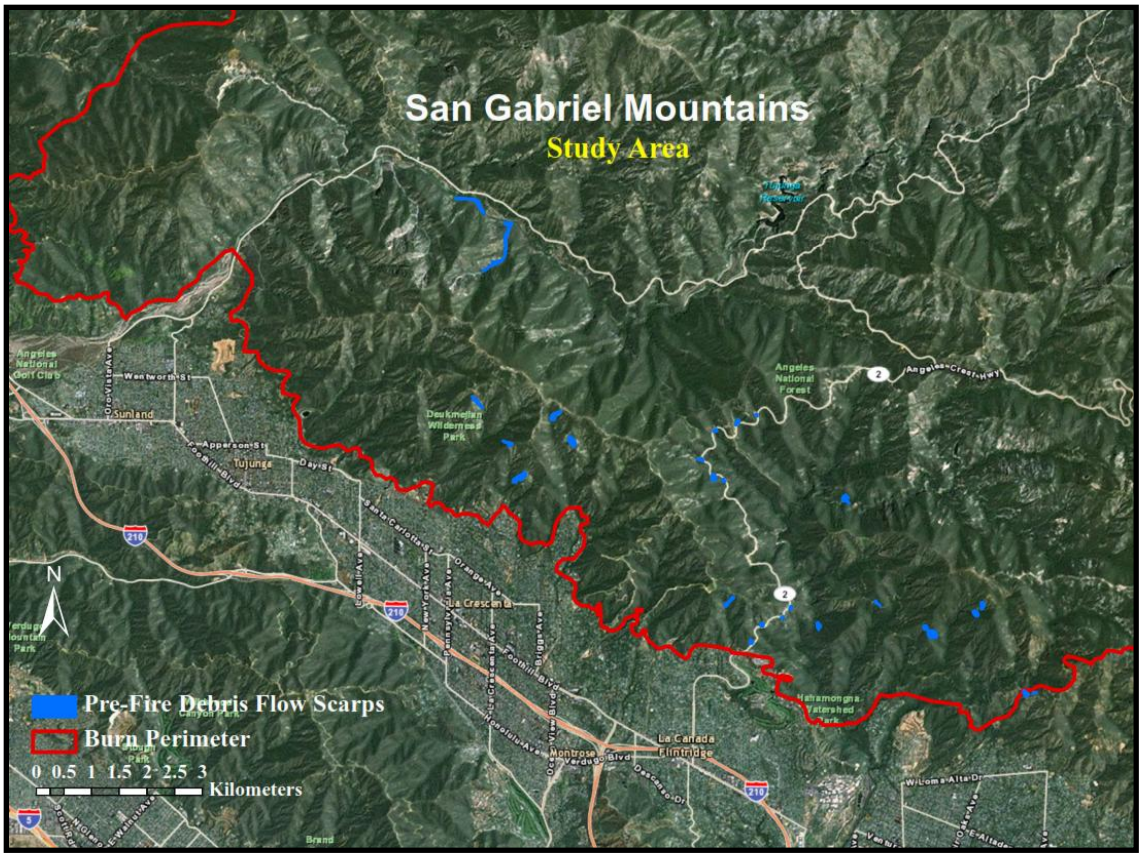

Figure 11. Aerial photograph with identified pre-fire debris flow boundaries (scarps) in the study area. Imagery is from the United States Department of Agriculture (USDA) National Agriculture Imagery Program (NAIP) imagery and enhanced versions of United States Geological Survey (USGS) Digital Ortho Quarter Quad (DOQQ) imagery.

Post-Fire Remote Imagery Mapping

In addition to the aerial photography previously mentioned, post-fire aerial photography was acquired from April-September 2010 from the National Agriculture Imagery Program (NAIP). This imagery is in four sections covering the burn area, see Table 3 for imagery information.

Post-fire imagery was added into ArcMap and a slope raster was rectified in ArcMap of the study area. Post-fire debris flows were identified by the same method as pre-fire debris flows mapped as polygons in ArcMap (Figure 12). The debris flow area (including the transportation, erosional areas and the deposition area) was calculated using the area calculation tool in ArcGIS. A comparison of the pre-fire and post-fire mapped debris flows determined any overlapping areas (Figure 13). Overlapping pre-fire debris flow scarps would indicate recent debris flows before the Station Fire. With no overlap, mapped post-fire flows are definitively the Station Fire debris flows. A KML file conversion to Google Earth was done to confirm the post-fire debris flow GPS locations (Figure 14).

Post-Fire Mapping

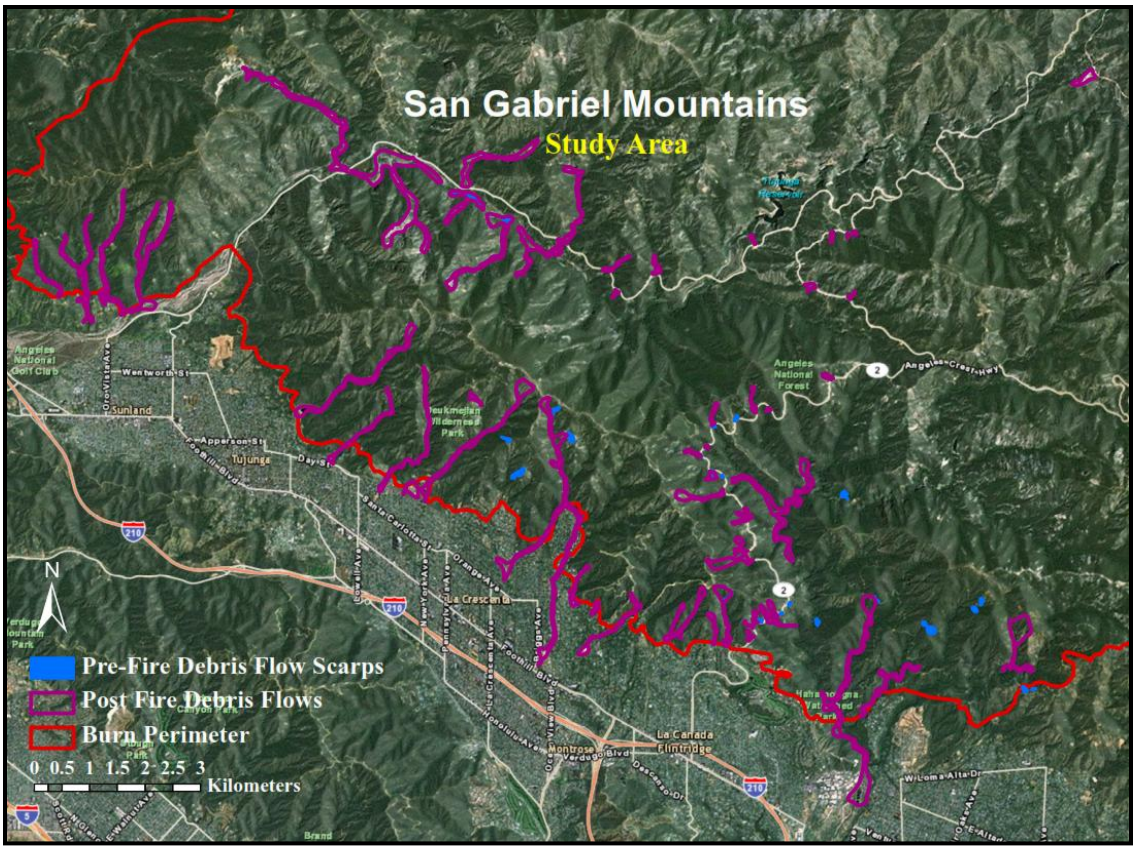

Figure 12. Aerial photograph with identified post-fire debris flows and pre-fire scarps. Imagery is from the United States Department of Agriculture (USDA) National Agriculture Imagery Program (NAIP) imagery and enhanced versions of United States Geological Survey (USGS)

Post-Fire Flows on Google Earth Map

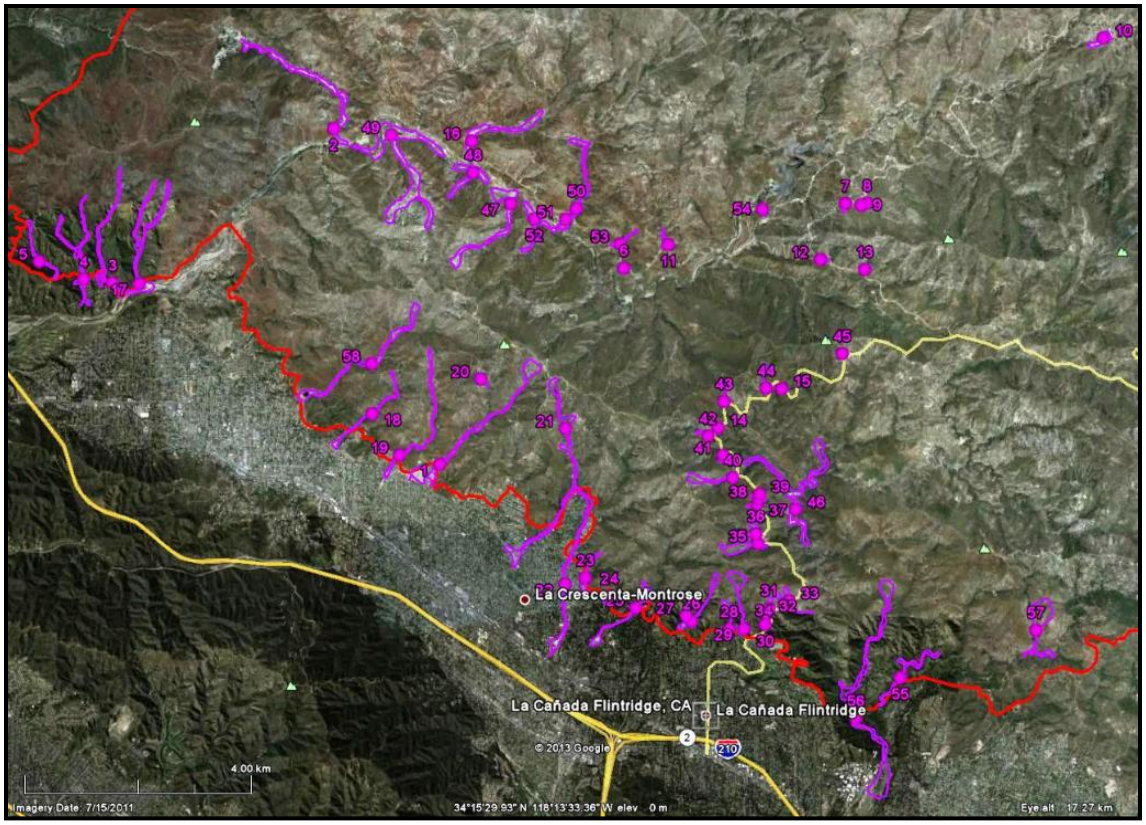

Figure 13. Google Earth map with labeled post-fire debris flows. Burn perimeter is in red; debris flows are outlined in purple.

Field Work

After GIS mapping of the post-fire debris flows on the aerial photos was completed, field work commenced. To prepare for the field work, the post-fire debris flow file from Google Earth was downloaded onto a GPS unit to insure accuracy in locating the debris flows in the field. Mapping from imagery revealed 58 debris flows. Only a small sample (16%) of these 58 debris flows were field mapped. They were chosen for easy accessibility and sample of flow sizes. Fourteen debris flows were field checked and of these, nine were measured for volumetric calculations (Table 4). The flows fell into three categories: 1) those that initiated on natural slopes and had undisturbed toes ("n/u": debris flows 2, 48, 49, and 52), 2) those that had initiated on natural slopes and flowed into an end debris flow basin ("n/b": debris flows 16, 22, 35, 43, 50, and 56), and 3) those that initiated on manmade (anthropogenic) slopes and had road fill for slopes and toes ("a/rf": debris flows 33, 34, 38, and 39). Photographs are located in the Appendix.

For each flow, lithologic characteristics and type of flow were determined and a grain size and a color analysis conducted (Table 4). This was done to ascertain if the flows were matrix-supported or clast-supported. Debris flows are classified as tilloids, which are matrix-supported sediment deposits with poor sorting.

Nine flows were chosen to measure their debris flow deposits: 2, 16, 22, 43, 48, 49, 50, 52, and 56. These were chosen for their accessibility and to achieve a reasonable population of the various sizes of flows. The deposits were measured by the following process. The location of the transition zone from erosion to deposition was noted using a GPS unit and was determined by the ending of the scouring and rilling of the bedrock to a

dumping of materials, typically at a slope between 8-10 degrees. From this transition point, a transect was measured down each edge of the flow to collect measurements, approximately every 30 meters. The depth of the deposition was recorded either along an exposed edge or by digging down to the basement. A transect down the middle of the flow was also conducted in the same manner. For the natural/undisturbed debris flows (n/u), direct measurements were obtained of the deposition. For the natural/into debris flow basin flows (n/b), it was measured where the deposition was before the debris flow basin clean out using the deposit marks along the edges of the flow and basin; the deposit removal lines could be clearly ascertained by recent gouge marks on the walls of the debris flow basins where the debris was removed. Debris flows 22, Pickens Canyon, and 56, Arroyo Seco, have debris flow gates to slow down the debris flows. Some of these gates trapped debris and several gates broke, trapping some material. All basins were cleared out either to the concrete base (22 and 56) or to the ground (43 and 50). The debris flow deposits were removed by the Los Angeles County Department of Public Works (LACDPW) prior to this investigation (Sediment Management, 2013).

To assess accurately the origination of the debris flow material, the drainage area for each remotely mapped debris flow was mapped onto Arcmap (Figure 15). The drainage area was ascertained by the area around each debris flow, which contributed to the debris material. This area included the debris flow erosional area, as dry ravel and other materials had accumulated into the channels from the fire, and did not include the debris flow deposition area. Utilizing the slope map and the field work information that at an 8-10° slope deposition commences, the drainage areas were mapped to this channel slope angle and the deposition areas began at this slope angle.

DEBRIS FLOW CHARACTERISTICS

DEBRIS FLOW ID	LITHOLOGY OF CLASTS	ROUNDNESS	MATRIX COLOR	GRAIN SIZE PERCENTAGES	DEBRIS FLOW TYPE*
2	Granite, gneiss, granodiorite, altered conglomerate, quartz diorite	Sub-angular, poorly sorted	Pale brown 5YR 5/2	15% boulders, 25% cobbles, 25% pebbles, 35% sand	n/u
16	Granite, gneiss, granodiorite, quartz diorite, pink feldspars	Sub-angular - sub-rounded, poorly sorted	Pale brown 5YR 5/2	5% boulders, 10% cobbles, 35%, pebbles, 50% sand	n/b
22	Granite, gneiss, granodiorite, quartz diorite, pink feldspars	Angular - sub-angular, poorly sorted	Pale brown 5YR 5/2	15% boulders, 15% cobbles, 30% pebbles, 40% sand	n/b
33	Colluvium fill: Granite, schist clasts, gneiss	Sub-angular - sub-rounded, poorly sorted	Grayish brown 5YR 3/2	5% boulders, 15% cobbles, 30% pebbles, 50% sands	a/rf
34	Colluvium fill: Granite, schist clasts, gneiss	Sub-angular - sub-rounded, poorly sorted	Grayish brown 5YR 3/2	5% boulders, 15% cobbles, 30% pebbles, 50% sands	a/rf
35	Granite, gneiss, granodiorite, quartz diorite, pink feldspars	Angular - sub-angular, poorly sorted	Med. Brown 5YR 3/4	15% boulders, 15% cobbles, 30% pebbles, 30 % sands	n/b
38	Colluvium fill: Granite, schist clasts, gneiss	Sub-angular - sub-rounded, poorly sorted	Grayish brown 5YR 3/2	5% boulders, 15% cobbles, 30% pebbles, 50% sands	a/rf
39	Colluvium fill: Granite, schist clasts, gneiss, granodiorite	Sub-angular - sub-rounded, poorly sorted	Grayish brown 5YR 3/2	5% boulders, 15% cobbles, 30% pebbles, 50% sands	a/rf
43	Granite, schist clasts, gneiss	Angular - sub-angular, poorly sorted	Med. Brown 5YR 3/4	0% boulders, 40% cobbles, 30% pebbles, 30 % sand	n/b
48	Granite, gneiss, granodiorite, quartz diorite, pink feldspars	Angular - sub-angular, poorly sorted	Pale brown 5YR 5/2	15% boulders, 25% cobbles, 25% pebbles, 35% sand	n/u
49	Granite, gneiss, granodiorite, quartz diorite, pink feldspars	Angular - sub-angular, poorly sorted	Pale brown 5YR 5/2	15% boulders, 25% cobbles, 25% pebbles, 35% sand	n/u
50	Granite, gneiss, granodiorite, quartz diorite, pink feldspars	Angular - sub-angular, poorly sorted	Pale brown 5YR 5/2	10% boulders, 25% cobbles, 35% pebbles, 35% sand	n/b
52	Granite, gneiss, granodiorite, quartz diorite, pink feldspars	Angular - sub-angular, poorly sorted	Pale brown 5YR 5/2	15% boulders, 25% cobbles, 30% pebbles, 35% sand	n/u
56	Granite, gneiss, granodiorite, quartz diorite, pink feldspars	Angular - sub-angular, poorly sorted	Pale brown 5YR 5/2	10% boulders, 20% cobbles, 35% pebbles, 35% sand	n/b

* n/u = natural debris flow/undisturbed, n/b = natural debris flow/into debris flow basin, a/rf = anthropogenic/road fill

Table 4. Field checked debris flow characteristics (measured flows are highlighted).

Debris Flow Drainage Areas and Deposition Areas

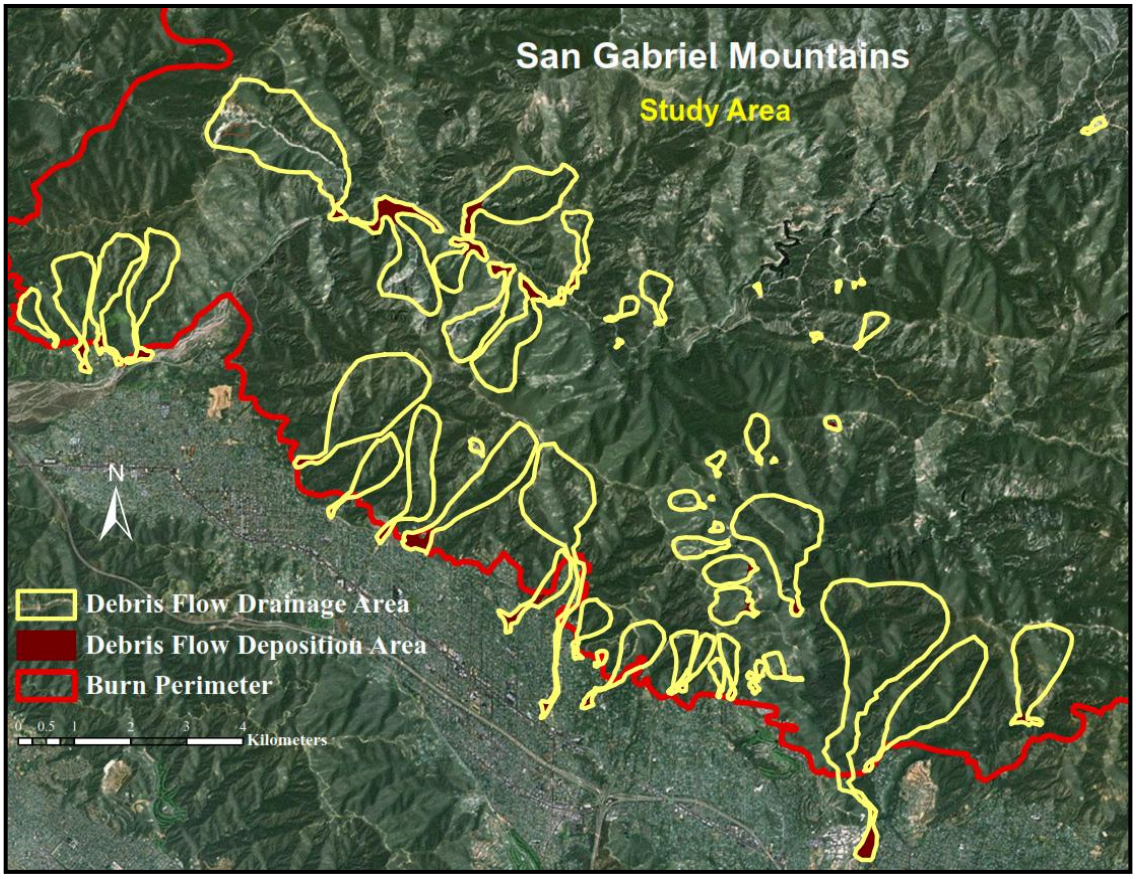

Figure 14. Aerial photograph with mapped debris flow drainage areas and deposition areas. Imagery is from the United States Department of Agriculture (USDA) National Agriculture Imagery Program (NAIP) imagery and enhanced versions of United States Geological Survey (USGS) Digital Ortho Quarter Quad (DOQQ) imagery.

Volume Calculations

After collecting the field data, the GPS coordinates for the depth measurements for each measured debris flow were recorded in ArcMap (and onto a Google Earth map for confirmation that the mapped flows were actual flows) with the mapped debris flows. Each flow was separated into discreet trapezoidal sections (Figure 16) and the volume of each section was calculated. All sections were added together to provide a total volume of debris. The average depth of each flow segment was used in the calculations. Figures 17 and 18 show an example volume calculation for debris flow 50. Equation 5.1 is the trapezoid volume equation. Equation 5.2 is the volume of deposition at the rounded toe or basin equation (Mathzone, 2013).

Equation 5.1. Trapezoid volume equation:

$V = [(W1+W2)/2*((D1 +D2)/2]*L$

W1 = length of the top
W2 = length of the bottom
D1 = deepest measured depth (height of debris flow)
D2 = shallowest measured depth (height of debris flow)
L= length of the trapezoid (the distance between W1 and W2

Equation 5.2. Volume of deposition at the rounded toe or basin equation:

$V = D* ((2*C *H /3) + (H^3/2*C))$

D = measured depth of debris flow
C = length of the chord
H = height of arced portion of the circular segment

Sketch of Volume Calculations

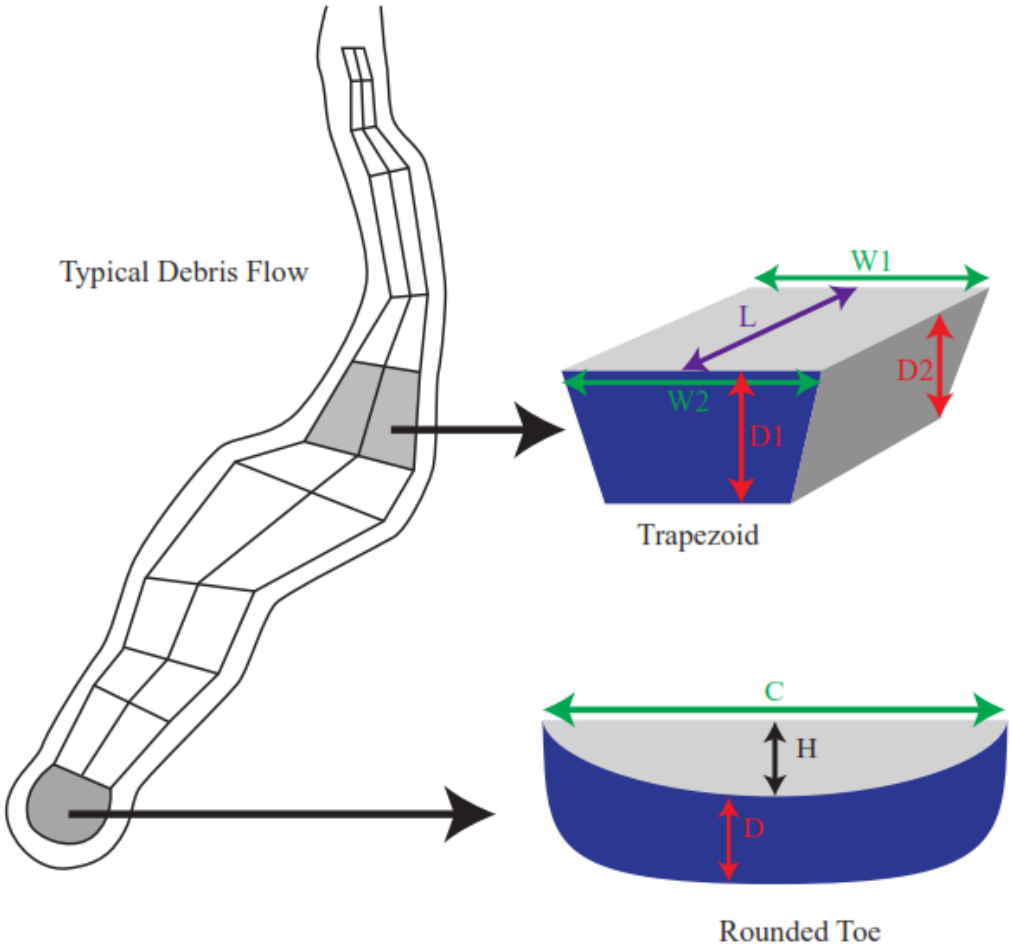

Trapezoid V = [(W1+W2)/2*((D1 +D2)/2]*L

W1 = length of the top
W2 = length of the bottom
D1 = deepest measured depth (height of debris flow)
D2 = shallowest measured depth (height of debris flow)
L= length of the trapezoid

Rounded Toe V= D* ((2*C *H /3) + (H3/2*C))

D = average measured depth of debris flow
C = length of the chord
H = height of the segment (arced portion)

Total Debris Flow V = Total Trapezoid Volumes + Rounded Toe Volume

Figure 15. Schematic sketch of debris flow volume calculations. Debris flow deposition calculations involved adding several trapezoid volumes to an end segment volume.

Field Measurements

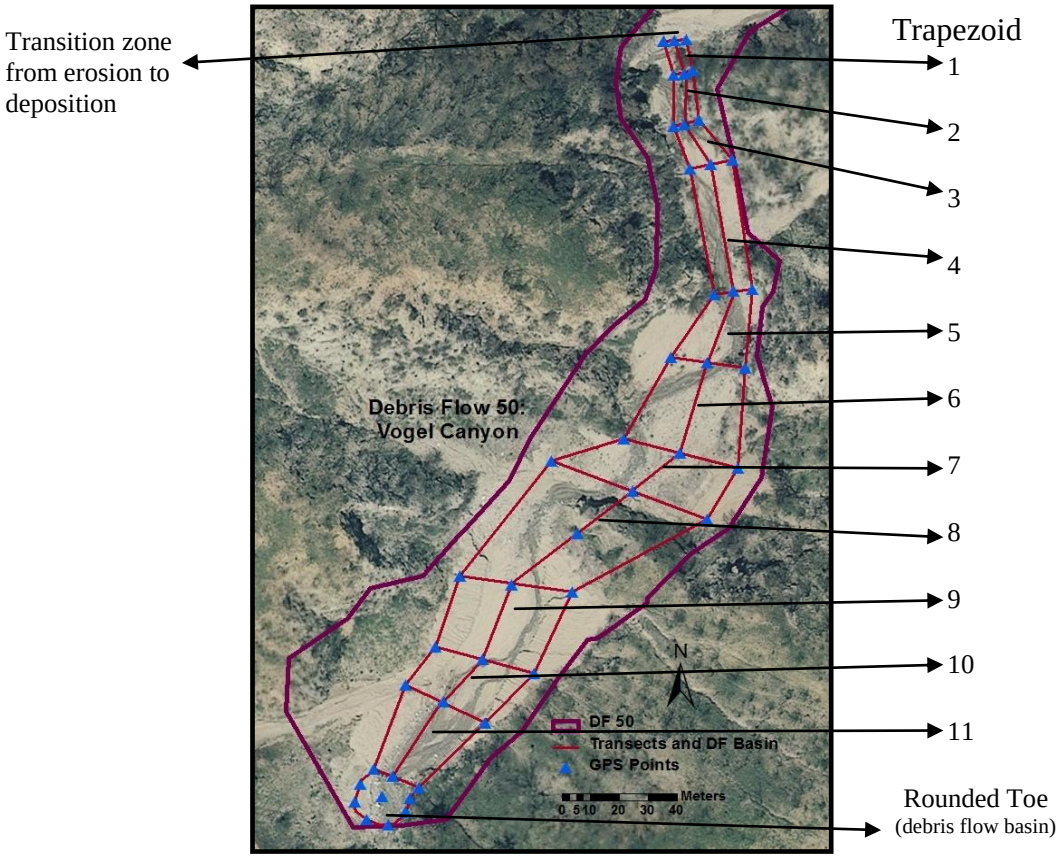

Figure 16. Measured transects and debris flow basin down debris flow 50 (Vogel Canyon) with GPS points

Volume Calculations

Trapezoid	1	2	3	4	5	6	7	8	9	10	11	Total Trap. V(m^3)
W1 (m)	8.2	9.9	9.1	15.5	13.4	26.3	41.0	58.3	39.5	23	30.8	
W2 (m)	9.9	9.1	15.5	13.4	26.3	41.0	58.3	39.5	23	30.8	17.6	
L (m)	13.3	17.1	17.0	46.2	26.4	28.3	20.7	53.0	28.3	20.7	32.3	
D1 (m)	1.8	0.6	0.9	1.2	1.7	1.5	2.1	0.8	1.1	0.8	3.5	
D2 (m)	1.0	0.8	1.5	1.5	1.6	1.9	1.5	1.8	2.8	3.5	4.0	
Volume (m^3)	168.0	113.9	255.5	897.9	866	1637.9	1839.7	3330.3	2053.7	1493.6	2931.2	15586.5

Chord (m)	Height (m)	Avg. Depth (m)	V of Rounded Toe (m^3)
16.0	2.0	2.0	46

Total Trapezoid V + V of Rounded Toe = V of DF 50
15,586.5 m^3 + 46 m^3 = 15,629.7 m^3
TOTAL VOLUME = 15,630 m^3

Figure 17. Debris flow volume calculations for debris flow 50

Standard Error Analysis

In order to validate the data and results, a standard error analysis was performed to determine the standard error for each measurement. The estimated standard error for the flow area measurements in ArcMap is ±10% according to the ArcGIS Resource Center. For the standard error of the volume of each flow, the formula for standard error was utilized when combining measurements by multiplication or division (in a product of measured quantities, relative errors add in quadrature). In that case, δ_x denotes error in quantity x and assuming that x and y and their errors δ_x and δ_y are measured independently. Also, $z = xy \Rightarrow \delta z/z$, z is the product of x and y and where δ_z is the total relative and percent error (Notes, 2013). Equation 5.3 defines the percent error and Equation 5.4 is the standard error equation for this project.

Equation 5.3. Percent error equation:

$$\frac{\delta_z}{z} = \sqrt{\left[\frac{\delta_x}{x}\right]^2 + \left[\frac{\delta_y}{y}\right]^2}$$

Equation 5.4. Standard error equation:

$$\delta_{flow} = \left(\sqrt{\left[\frac{\delta_{area\ T}}{area\ T}\right]^2 + \left[\frac{\delta_{avg\ flow\ depth}}{avg\ flow\ depth}\right]^2} \right) V_{flow}$$

area T = total area of a given flow

$\delta_{area\ T}$ = standard error of a given flow's area measurement

avg flow depth = average depth of a given flow

$\delta_{avg\ flow\ depth}$ = standard error of the average depth of a given flow

V_{flow} = volume of a given flow

δ_{flow} = standard error of a given flow's volume calculation

Chapter 7: Results

Mapping

Arc GIS mapping of the pre-fire aerial photographs revealed 27 pre-fire debris flows and/or landslide scarps in the study area (Figure 11). Post-fire mapping from aerial photographs revealed 58 new debris flows generated after the Station Fire and subsequent winter rains (Figure 12). Of these 58 debris flows, only four occurred over previously mapped scarps. On average, one debris flow occurred for every 2 km^2. The combined drainage area of all the debris flows amounts to 6% of the total study area (192 km^2).

Debris Flow Characterization

Typical debris flow clasts consist of: granite (some with large pink feldspars), gneiss, granodiorite, and some anorthosite and gabbro. Grains are typically sub-angular and poorly sorted. The most common matrix color is pale brown (5YR 5/2). Grain size percentages averaged for all field-checked flows are: 7% boulders, 19% cobbles, 30% pebbles, and 44% sand (Table 4). All debris flows are matrix-supported, in which the clasts (boulders and cobbles) are supported within the fabric of the pebbles and sand. Debris flows are classified as matrix-supported and poorly sorted and this analysis determined that these flows were definitely debris flows and not mudflows or granular flows.

Debris flows run-out lengths (measured from the initiation of the debris flow to the debris basin or toe) averaged 1.2 km. The largest debris flow run-outs were between 2.7 and 3.7 km and the smallest were between 0.2 and 0.4 km.

Regression Analysis

A regression analysis using the new volume calculations was used to determine the relationship between debris flow drainage area and the debris flow depositional volumes. This regression analysis gives an estimate of the amount of debris flow deposition given a debris flow drainage area and revealed a linear relationship between the debris flow drainage area per flow covered by the debris flow and the volume of deposition per each flow (Figure 19). Equation 6.1 fits the observed correlation in a linear relationship ($R^2 = 0.94$). Equation 6.2 also fits the observed correlation in an exponential relationship ($R^2 = 0.93$). Both regression expressions (linear and exponential) have excellent accuracy.

Equation 6.1. Linear regression equation:

$V = (0.053 \pm 0.01)A$

Equation 6.2. Exponential regression equation:

$V = 8059.4e^{1E\text{-}06A}$

A = debris flow drainage area per debris flow (m^2)

V= total volume of deposition per debris flow (m^3)

A comparison of these two equations (Equation 6.1 and Equation 6.2) for the data set reveals, for this project, the linear regression (Equation 6.1) is a superior match to determine the data analysis for the volume calculations. For example, using the linear equation for debris flow 13 (A = 7,832 m^2) the calculated deposition volume is 415 ± 62 m^3 (Table 5). This size deposition volume for this size drainage area is consistent with the

field data. However, using the exponential equation for debris flow 13 (A = 7,832 m^2), yields the calculated deposition volume of 8,123 ± 1,218 m^3. This deposition value is too high for such a small drainage area, according to the field data. For the ten debris flow drainage areas under 20,000 m^2 (17% of the debris flow drainage areas), similar high volumes occur when using the exponential equation (Equation 6.2). Consequently, the exponential regression equation when extrapolated beyond the data set for the smaller debris flow drainage areas is not an accurate assessment of the debris flow volumes deposited. Thus, the linear equation (Equation 6.1) better represents the field data.

The calculations for the total volume of deposition per flow for debris flows not field measured using the linear equation (Equation 6.1) are in Table 5. Table 6 illustrates the mapped debris flow drainage areas and measured debris flow volumes and differentiates between the natural debris flows into undisturbed basins (n/u) and the natural debris flows into man-made debris flow basins (n/b).

Debris Flow Drainage Area vs. Debris Flow Volume

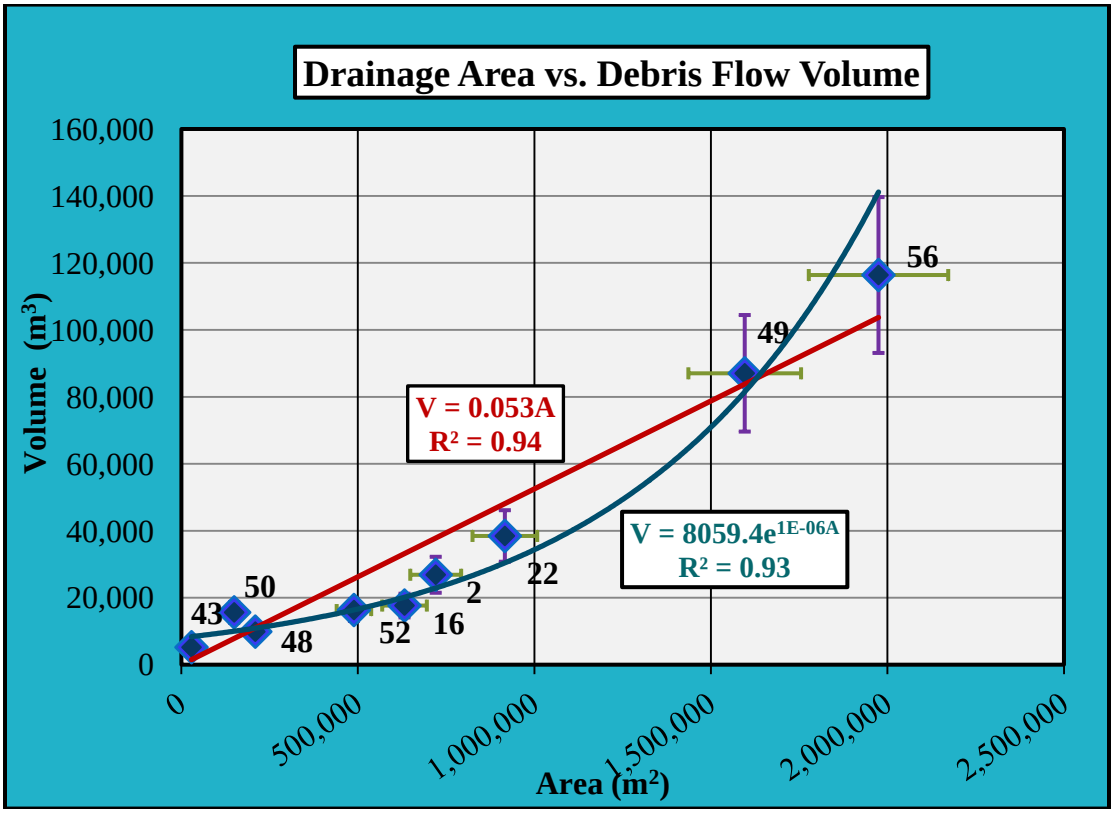

Figure 18. Debris flow drainage area vs. debris flow deposition volume showing linear regression relationship in red line and exponential regression relationship in green curved line with standard error bars.

Debris Flow Drainage Area and Debris Flow Volume Chart

Debris Flow ID	Drainage Area in m^2	Field Measured Volume (m^3)	Calculated V (V = 0.053 Area) (m^3)	Debris Flow ID	Drainage Area in m^2	Field Measured Volume (m^3)	Calculated V (V = 0.053 Area) (m^3)
1	583,269		30,913±4,637	30	21,663		1,148±172
2	720,472	26,864± 7269		31	34,001		1,802±270
3	273,824		14,513±2,177	32	8,833		468±70
4	321,912		17,061±2,559	33	74,815		3,965±595
5	98,376		5,214±782	34	81,675		4,329±649
6	12,422		658±99	35	234,927		12,451±1,868
7	14,166		751±113	36	68,931		3,653±548
8	9,684		513±77	37	42,558		2,256±338
9	3,330		176±26	38	27,420		1,453±218
10	129,986		6,889±1,033	39	16,971		899±135
11	36,180		1,918±288	40	156,536		8,296±1,244
12	36,952		1,958±294	41	46,019		2,439±366
13	7,832		415±62	42	30,702		1,627±244
14	5,917		314±47	43	31,363	5,160± 1,253	
15	6,330		335±50	44	35,456		1,879±282
16	632,135	17,669± 5,698		45	24,333		1,290±193
17	470,988		24,962±3,744	46	737,515		39,088±5,863
18	141,773		7,514±1,127	47	479,890		25,434±3,815
19	240,334		12,738±1,911	48	284,805	9,878± 2,098	
20	41,432		2,196±329	49	1,595,775	87,023± 31,238	
21	660,656		35,015±5,252	50	149,590	15,630± 5,275	
22	972,038	38,456± 8,440		51	79,558		4,217±632
23	83,384		4,419±663	52	488,845	16,329± 5,769	
24	27,327		1,448±217	53	48,118		2,550±383
25	158,229		8,386±1,258	54	11,060		586±88
26	133,584		7,080±1,062	55	195,713		10,373±1,556
27	31,422		1,665±250	56	1,974,665	116,377± 38,483	
28	55,460		2,939±441	57	490,696		26,007±3,901
29	219,530		11,635±1,745	58	490,484		25,996±3,899

Table 5. Debris flow drainage area (calculated from ArcGIS mapping) and debris flow volume (field measured and calculated from linear regression). Field measured flows are highlighted in blue.

Mapped Debris Flow Drainage Areas and Measured Debris Flow Deposition Volumes

Debris Flow ID	Remote Mapped Debris Flow Drainage Area in m^2	Field Measured Volume in m^3
2 (Gold Canyon)	720,472 ± 72,050	26,864 ± 7269
16 (Ybarra Canyon)	632,135 ± 63,220	17,669 ± 5,698
22 (Pickens Canyon)	916,320 ± 91,630	38,456 ± 8,440
43 (Dark Canyon)	28,815 ± 2,880	5,216 ± 1,170
48 (small canyon tributary east of Delta Canyon)	209,400 ± 21,000	9,878 ± 2,098
49 (Delta Canyon)	1,595,775 ± 159,600	87,023 ± 31,238
50 (Vogel Canyon)	149,590 ± 15,000	15,630 ± 5,275
52 (Stone Canyon)	488,845 ± 49,000	16,329 ± 5,769
56 (Arroyo Seco Canyon)	1,974,66 ± 197,500	116,377 ± 38,483

Table 6. Remote mapped debris flow drainage areas and measured debris flow deposition volumes. Natural debris flows into undisturbed basins (n/u) are highlighted in purple; natural debris flows into man-made debris flow basins (n/b) are highlighted in gray.

The R^2 value (coefficient of determination, defined as the ratio of the sum of squares explained by a regression model), the overall accuracy of the linear regression, is:

$R^2 = 0.94$.

The adjusted R^2 (adjusts for the number of explanatory terms in a model relative to the number of data points and is useful when the R^2 is based on a sample, not the entire data set, as in this study) is:

Adjusted $R^2 = 0.94$.

The R^2 and Adjusted R^2 values indicate that there is a 94% probability that this linear regression is accurate for the sample data set (the nine measured flows).

The standard error from the linear regression (the estimated standard deviation of the error of the process by which it is generated, or the estimate of the standard deviation around the line - a measure of how much the volumes vary for a given area value) is:

Standard Error = $9914m^3$.

The Standard Error value indicates that the measured volumes vary around the linear regression at $\pm 9914m^3$.

The Significance F value, the probability that the regression is not random (the smaller the number the greater probability that the regression is not random) is:

Significance F = 1.4×10^{-5}.

This Significance F value indicates that this linear regression is not random, but is significant.

The P-values for the y-intercept, indicative of reliability (the smaller the number the greater the reliability) are respectively:

Y-intercept: P-value = 0.35

Area: P-value = $1.4 \times 10^{-5} \approx 0.0$

Since the P-values are small, there is a greater reliability for this linear regression (Table 7).

Regression Analysis

Summary Output

Regression Statistics	
Multiple R	0.97
R Square	0.94
Adjusted R Square	0.94
Standard Error	±9914 m^3
Observations	9

Intercept	*P-value*
Drainage Area (m^3)	1.4×10^{-5}

ANOVA

	df	*SS*	*MS*	*F*	*Significance F*
Regression	1	11,223,303,775	11,223,303,775	114.1953	1.4×10^{-5}
Residual	7	687,971,441	98,281,634		
Total	8	11,911,275,216			

Table 7. Regression analysis: summary output and ANOVA (significant columns and rows are highlighted). A R^2 and adjusted R^2 values of 96% and 95% indicate the accuracy of the regression. The Standard Error, a measure of how much the volumes vary for a given area value, is ±8231.7 m^3. The Significance F value, the probability that the regression is not random (the smaller the number the greater probability that the regression is not random) is 3.73×10^{-6}. The df value is the degrees of freedom. The SS value is the calculated sum of squares. The MS value is the mean square terms. The P-values are small: there is a greater reliability for this linear regression.

Volume Analysis

Having determined the best fit equation, the estimated volume of deposition for each flow not measured in the field was calculated using the linear coefficient from the regression analysis (Table 8). The percentage of the study area covered by the debris flows was calculated and is 6%.

Erosion Analysis

Dividing percentage of the study area covered by the debris flows (6%) by the total erosion in meters, the total fire erosion (mm/yr) due to these flows in the study area was calculated. In addition, the debris flow erosion rates for the debris flows were calculated. Finally, the erosion rates for a 30 year fire reoccurrence and a 50 year reoccurrence were calculated (Table 9). These rates were chosen based on the fire history in the San Gabriel Mountains (Hellmers, 1962; Keeley and Fotherington, 2001; Lavé and Burbank, 2004; and Cannon et al., 2010). A comparison the 30 year frequency erosion rates to those of Lavé and Burbank (2004) is shown in Table 10.

Geomorphologic Results

Several geomorphologic features were identified with these post-fire debris flows. All field checked debris flows had rilling and scour marks in the erosional channel sides of the debris flow channel walls. The larger debris flows (debris flows: 2, 49, 50, and 56) had more extensive rilling and scour marks. All field checked flows were matrix-supported flows. All natural/undisturbed flows, n/u, (debris flows: 2, 48, 49, and 52) had boulders deposited all the way to the edge of the flow deposit terminus and had fan-like toe deposits which spread out at the lowest point of the deposition area and overflowed their water catchments.

The post-fire debris flows that were field mapped represent the most recent of a continuum of repeating debris flows in the San Gabriel Mountains, as shown in Figure 6a in the Appendix (debris flow 49). This figure shows the state of the most recent flow in relation to the past debris flow deposits. These recent post-fire flows appear to be commensurate with past flows. Debris flows 2 and 48 also had substantial older debris flow deposits up to 3 meters in height.

Results Compilation

In the total study area (192 ± 1.9 km^2), debris flows covered 8.9 ± 0.90 km^2. The total volume of debris flow deposition is 717,300 ± 179,310 m^3 (Table 8). Fifty-four of 58 GIS mapped debris flows are new (93%) and have a spatial distribution of one flow per every 2 km^2. The erosion per m^2 in each debris flow drainage area is 670 ± 134 mm/m^2. Debris flow deposition began on approximately a slope of 8-10° at the base of each debris flow drainage area. Using the frequency of a 30 year occurrence (Hellmers, 1962; Keeley and Fotherington, 2001; Lavé and Burbank, 2004; and Cannon et al., 2010), the debris flow erosion rate for the total burn area is 0.13 ± 0.02 mm/yr, averaged over the entire burn area. Within the debris flow drainage areas, the erosion rate is much higher at 22 ± 4.3 mm/yr (Table 9). Using the frequency of a 50 year occurrence, the debris flow erosion rate for the total burn area is 0.075 ± 0.01 mm/yr, averaged over the entire burn area. Within the debris flow drainage areas, the erosion rate is much higher at 13 ± 2.6 mm/yr (Table 9). The linear coefficient of debris flow drainage area vs. debris flow volume is $V = (0.053 \pm 0.01)A$.

Area and Volume Calculations

Total Study Area in km^2	Total Debris Flow Drainage Area in km^2	Debris Flow Drainage Area as % of Study Area	Total Volume of Debris Flow Deposition in m^3
192 ± 1.9	1.1 ± 0.12	6	717,300 ± 179,310

Table 8. Area and volume calculations: total study area, total flow area, percentage of flow area, and total volume of deposition.

Calculated Area Erosion by Frequency (every 30 or 50 years)

	30 years	50 years
Erosion Burn Area mm/freq = mm/yr	0.13 ± 0.02	0.075 ± 0.01
Erosion Debris Flow Drainage Area mm/freq = mm/yr	23 ± 4.3	13 ± 2.6

Table 9. Calculated erosion due to debris flows for the total burn area and for the total debris flow area by a frequency of 30 or 50 year occurrence.

Comparison of Erosion Rates in San Gabriel Mountains

COMPARISON OF EROSION RATES		
DEBRIS FLOW EROSION RATE (30 yr event): AVERAGED OVER TOTAL STUDY AREA	DEBRIS FLOW EROSION RATE (30 yr event): WITHIN DEBRIS FLOW DRAINAGE AREAS	DEBRIS FLOW BASIN AND DAM MEASUREMENTS EROSION RATE (Lavé and Burbank, 2004)
0.13 ± 0.02 mm/yr	22 ± 4.3 mm/yr	0.9 - 1.6 mm/yr

Table 10. Comparison of erosion rates for a 30 year event.

Chapter 8: Discussion

Implications for Overall Erosion

The hypothesis of this project is that post-fire debris flows in the San Gabriel Mountains are responsible for a disproportionate amount of total erosion in any given debris flow drainage area 1-2 years after a burn. This study demonstrates that post-fire debris flows, although covering only 6% of the San Gabriel Mountains, are important contributors to the erosion rates immediately after a large burn. Furthermore, this study reveals that post-fire debris flow erosion rates (Tables 9 and 10) do contribute to the overall erosion rates of the San Gabriel Mountains. If debris flows after the Station Fire are representative of the typical large fire that occurs in the region, they account for about 8 - 14% by volume of total deposition after fires.

Given a debris flow drainage area and no other available data, this empirical data analysis suggests the volume of deposition can be quantitatively determined based on the regression coefficient of

$$V = (0.053 \pm 0.01)A.$$

This linear coefficient is noteworthy in that it is derived from a recent fire and is not based on a predicted model analysis. According to the U.S. Corps of Engineers (Gatwood et al., 2000) and the Los Angeles County of Public Works (Sedimentation Manual, 2006), in canyons containing debris flow areas under 1 million km^2 in southern California, which includes most debris flow drainage areas in this project, a linear regression coefficient is expected.

Fire Data

Recent documented fires in the San Gabriel Mountains with post-fire debris flows include: the 1927 Fire, the 1933 Pickens Canyon Fire, the 1969 Fire, the 1975 Middle Fire, the 1977 Mill Canyon Fire, the 2005 Harvard Fire, the 2007 Barham Fire, and the 2008 Santa Anita Fire, as well as the 2009 Station Fire. Over the last century, small fires and post-fire debris flows occur approximately every 9 years, medium fires with post-fire debris flows occur approximately every 15 years, and large fires, such as the Station Fire, with post-fire debris flows occur approximately every 20-30 years (Cannon et. al., 2010) (Figure 6). Keeley and Fotherington (2001) estimate that fire-rotation intervals average every 30-40 years in any given region in the California chaparral areas. Hellmers (1962) estimates that each slope in the SGM is swept by fire every 30-50 years with resulting debris flows. In southern California, the recurrence interval for medium to large fires has increased from a natural level of every 65-100+ years, based on charcoal studies, to approximately every 20 years in modern times owing to the impact of humans on fire frequency (Alexander, 1999). The results of this study reveal that post-fire debris flows may be more important contributors to the total erosion in the San Gabriel Mountains during modern times than a century ago, due to the increase of wildfires.

Comparison with Studies Done in SGM and Western United States

Based on records of the infilling of debris flow basins on the southern front of the San Gabriel Mountains from 1928 to 1988, Lavé and Burbank (2004) calculated erosion rates averaging from 0.9 to 1.6 mm/yr from the infilling of debris flow basins on the southern front of the San Gabriel Mountains landscape. They suggest that fire related debris flows may account for approximately 10% of the denudation in the SGM. This

project's findings confirm their results, assuming a 30 year recurrence, and have an erosion rate of 0.13 ± 0.02 mm/yr, which is 8-14% of their total erosion rate.

A study of catchment-averaged, millennial-scale erosion rates across the San Gabriel Mountain range conducted using detrital cosmogenic ^{10}Be analysis revealed an erosion rate of 0.035 - 1.1 mm/yr (DiBiase et al., 2009). Channel steepness was found to be a reliable topographic metric of erosion rate in actively deforming orogens when sedimentary sequences suggest deposition occurs simultaneously with tectonism, based on their average erosion rate. The erosion results of this project fall well within the results of DiBiase et al. (2009) at 0.13 ± 0.02 mm/yr for erosion due to debris flows, at a 30 year frequency.

This study confirms the analysis conducted by Warrick et al. (2012) in the Los Padres National Forest, California (as well as others including Cannon et al., 2001, Cannon and DeGraff, 2009, and Kean and Staley, 2011) in which they found that wildfire followed by intense precipitation produces annual sediment yielding much greater deposition than expected without wildfire (Figure 2). They found that wildfires followed by heavy precipitation are shown to produce annual sediment yields that are a magnitude greater than expected without wildfires. The combination of fires and post-fire debris flows was demonstrated to occur at 30 yr recurrence intervals, and sediment discharge from these sporadic events is significant to landform evolution, geomorphology, and rates and styles of sedimentation within the geologic record. Their results are similar to the results of this study, as the intense rains following the Station Fire occurred due the El Nino event that winter causing the large post-fire debris flows.

Previous studies in the western United States have developed prediction models for the probability of occurrence and volume of post-fire debris flows. Cannon et al. (2010) developed five models describing debris-flow volume as a function of basin gradient, aerial burn extent, and storm rainfall from a study on 56 basins burned by eight fires in the western United States. The probability models were tested on the 2003 Hot Creek Fire in central Idaho in which they identified basins that are most susceptible to large debris flow events. Only two of the five models gave useful predictions of post-fire debris flow volumes. They concluded that their probability models require further refinement based on physical evidence, such as the results of a study. This study gives empirical results to help confirm a model's predictions.

In a study conducted in southern California on nine debris basins, Rulli and Rosso (2005) developed a physically based simulation model to predict the sediment deposits from burned and unburned catchments. Their model revealed that sediment production increases from approximately 7 to 35 times after a wildfire. This study differs from theirs, Rulli and Rosso (2005), in that this study is based on field collected data from 1 burn event and the ensuing post-fire debris flows; however, it is similar in that this study reveals that sediment production increases by approximately 5 times after a fire, assuming a 30 year recurrence.

Comparison with Global Studies

Nyman et al. (2011) recently established that post-fire debris flows are a significant erosional process in southeast Australia and quantified erosion rates in a small (< 5 km^2) area with steep headwater catchments. Their paper is the first to document the occurrence of post-fire debris flows in Australia. Erosion rates calculated for this small

catchment are 4.6 ± 0.96 mm to 18.4 ± 2.7 mm/event (mm/yr) for 13 post-fire debris flows (Nyman et al., 2011). Their erosion rate, within the debris flow channel areas, is smaller than this project's erosion rate (23 ± 4.3 mm/yr) conducted on the post-fire debris flow drainage channels in the San Gabriel Mountains, probably due to differences in the slope steepness, materials, tectonic activity, type of vegetation and other factors; only the climate is similar.

Studies have reached similar results in other regions of the world with comparable Mediterranean climates; however, they lack the detailed quantitative data analysis that this study provides. In 2006, post-fire debris flows in Portugal caused considerable erosion; however, no quantitative data were published. Lourenço et al. (2012) concluded that further data collection, analysis, and methods to quantify potential hazards are necessary to comprehend post-fire hazard assessment.

Santi and Morandi (2012) compared debris flow volumes from unburned and burned areas in the Italian Alps, the Pacific Northwest, and the western United States. Their findings reveal that within 1 year of a burn the debris flows are up to 5.4 times greater than unburned areas and the Western U.S. has larger debris flows than those in the Italian Alps and the Pacific Northwest. Their analysis revealed that there is a 5 times increase in debris flows the first year after a burn, which is typical of the San Gabriel Mountains (Cannon, et al., 2010).

In a study conducted in Taiwan using LiDAR-derived DTMs on landslide-induced sediment volumes from a typhoon event in 2009, in which several debris flows and mudslides occurred, Tseng et al. (2013) determined a relationship between landslide area and volume with the equation: $V=0.452A^{1.242}$ with $R^2= 0.91$ for disturbed areas (flow

areas) and $V=2.510A^{1.206}$ with $R^2= 0.96$ ($V=m^3$ and $A= m^2$) for landslide crown areas (top of scarps). The authors discuss that the volume data is most likely over or underestimated as these measurements were largely obtained from the LiDAR DTMs and very few were obtained from field measurements. As this project is field study for one event, the difference in magnitude between their study and this project may be attributed to the differing methods of analysis. The authors validated their data with 11 catchments outside the study area, in which they compared empirical data with their calculations from DTMs and the regression formula. This study confirms the importance of field measured debris flow drainage volumes when analyzing flow area vs. flow volume, which may be the reason this project's values are much lower than their study's values.

Larsen et al. (2010) used a compilation of landslide (rotational, translational, flow and avalanche failures in earth, debris and bedrock) measurements from over 4,000 global landslides to determine the volume-area relationship. These measurements were obtained from publications, digitized from published figures, and a few field measurements. The landslide volume to area data analysis showed a positive linear value of $y = 1.332 \pm 0.005x$ ($y=m^3$ and $x= m^2$) with $R^2 = 0.95$. In the study of the San Gabriel Mountains' landslides, they determined that episodic soil landslides (such as debris flows) reduce soil depths and increase bedrock weathering in proportion to their frequency. The post-fire debris flows following the Station Fire were observed to have increased the bedrock weathering as evidenced by the gouging and rilling in all field observed debris flow channels. The values from the study done by Larsen et al. (2010) are a magnitude higher than the values determined by this study and may be due to several factors. They studied multiple landslide types globally and this study focused on

the post-fire debris flows for one event; also, they utilized few field measurements and this project only utilized remote mapped and field mapped measurements.

Other Sources of Erosion in the SGM

Fire-induced sediment production is the foremost contributor to twentieth century erosion in the San Gabriel Mountains and represents 10-30% of the total erosion, according to Lavé and Burbank (2004). This project confirms their assertion and demonstrates that post-fire debris flows account for 8-14% of the overall erosion rate. The other percentage of erosion is caused by several factors: shallow landslides, soil slippages, wet and dry ravel, floods, fluvial incisions, rilling, soil mantle exfiltration (loss of water and soil from a drainage system), rock falls, mudslides, and deep-seated landslides (often tectonically induced) (Lavé and Burbank , 2004; DiBiase et al., 2010).

Study Error Analysis

According to the Los Angeles County Department of Public Works (2013) most of the debris flow basins and dams overfilled and poured into nearby roads (Highway 2 and Big Tujunga Road), neighborhoods, streets, and homes. This project measured the deposition volume of six of those debris flow basins, debris flows 16, 22, 43, 50, 52, and 56, which had already been emptied out prior to the field work (Table 4). Therefore, the volume calculations for these six debris flows are an underestimate of the sediment volumes generated by these flows. However, the volume calculations of the natural debris flows into undisturbed areas (n/u), debris flows 2, 48, and 49, are more representative of a typical debris flow sediment deposit (Table 4). The overall volume of deposition calculation from the post-fire debris flows (from the linear coefficient) is a probably a minimum value, especially for those flows which deposited into the man-made basins.

Another error consideration is the intense rainfall amounts from the El Niño event during the winter of 2009-2010. Intense and prolonged rains after a fire produce more post-fire debris flows than smaller storms. (Cannon et al., 2010; Warrick et al., 2012). During the winter of 2009-2010, after the Station Fire, several severe storms inundated the burnt steep, slopes of the San Gabriel Mountains (Figure 5). The rainfall amounts totaled over 760 mm; the average winter rainfall amounts are 560 mm (weatherspark.com, Los Angeles Almanac). Due to these immense rainstorms, there were more post-fire debris flows than anticipated (Cannon et al., 2011). This possibly caused more sediment deposition than an average rainfall year after a burn and may have skewed the results of this project.

Future Work

The findings of this project are limited to a single event, the post-fire debris flows after the Station Fire of 2009. Thus, another analysis should be done after an additional large fire and the subsequent post-fire debris flows in the SGM to analyze further the effect of post-fire debris flows on the erosion rates of the SGM. A study to determine the fire recurrence level for each individual canyon would also be beneficial.

Impact on Hazard Analysis

Most of the debris flow basins in the southeastern San Gabriel Mountains overflowed after the post-fire debris flows of the Station Fire and caused significant damage to personal and public property (BonTerra Consulting, 2010). Debris flow basins within the southwestern San Gabriel Mountains are cleaned out when they are at least 5% full of sediment. All debris flow basins in this study either had been cleaned out prior to the Station Fire, or were less than 5% full (Sediment Management, 2013).

This data analysis reveals a linear coefficient of 0.053 ± 0.01 for debris flow drainage area vs. sediment deposition volume for post-fire debris flows and demonstrates that, given a certain area in a burnt steep mountain terrain, the post-fire debris flows will produce a calculated sediment deposit. This value is useful in predicting the amount of sediment that may be deposited after debris flows in a burnt canyon with a debris flow in the SGM, is useful to assist in predicting debris volumes from post-fire debris flows, and is useful to for planning debris dam development and expansion. Using this simple regression analysis, this coefficient value could be utilized to help prevent damage to state, federal, and personal property by anticipating the debris volume expected and implementing hazard precautions for roads, populated areas, and biological environments affected by debris flows. This would potentially help save thousands of taxpayers' dollars in clearing away debris and the damages done to private and public property due to post-fire debris flows.

Conclusion

Post-fire erosion rates due to debris flows are calculated for the San Gabriel Mountains, as well as a correlation coefficient between debris flow drainage area and debris flow volume deposited. Map analyses and field measurements show that post-fire debris flows play an important erosion role in the SGM, the first year after a burn. These findings are consistent with previous studies showing that, within the first year after a fire, erosion rates range from 5 to 35 times greater than normal (Tan, 1998; Warrick et al, 2012: Santi and Morandi, 2012). Given a 30 year frequency of post-fire debris flows for a large-sized fire, the overall erosion rate is 0.13 ± 0.02 mm/yr and within the debris flow areas is 22 ± 4.3 mm/yr. Debris flows cover a mere 6 % of the San Gabriel Mountains in the study area, but these post-fire debris flows account for approximately 8-14% of the total erosion. Regression analysis of the debris flow drainage areas versus the debris flow deposition volumes reveals a positive linear correlation and suggests that as the area affected by a debris flow increases, so does the depositional volume of the debris flow. This linear regression has a correlation coefficient as expressed in: $V = (0.053 \pm 0.01)A$. Thus, given a debris flow drainage area in the SGM, or similar mountainous range with comparable climate, the expected volume is 0.053 ± 0.01 times the debris flow drainage area. The total volume of sediment produced by Station Fire post-fire debris flows in the 192 ± 1.9 km^2 study area is $717{,}300 \pm 179{,}310$ m^3. This empirical data analysis of post-fire debris flows is important in understanding the overall contributors to erosion rates in the SGM.

Post-fire debris flows caused changes to the geomorphology of debris flow areas. Within each debris flow drainage area, the debris flow erosional processes caused scouring and rilling in the channels and produced large sedimentary deposits into either a

debris flow basin or the debris flow toe. Most of the LA County debris flow dams overflowed into roads, neighborhoods, and homes after the debris flows subsequent to the Station Fire (Sediment Management, 2013). Natural undisturbed debris flows overflowed their water catchments and left massive deposits (debris flows: 2, 48, 49, and 52). Geomorphologic changes caused by post-fire debris flows are substantial to the debris flow areas.

These results suggest that in the SGM post-fire debris flows are significant contributors to overall erosion rates in burn areas within a year of the fire. The debris flow drainage area vs. debris flow volume regression equation from this study is noteworthy and useful to help predict the minimum sediment volumes from post-fire debris flows.

References

Ainsworth, Jack and Troy Alan Doss, 1995, Natural History of Fire and Flood Cycles, California Coastal Commission, Post-fire Hazard Assessment Planning and Mitigation Workshop at the University of California, Santa Barbara, Web 02/07/2013.

Alexander, David, 1999, Environmental Geology, Encyclopedia of Earth Science, Springer Netherlands, Web 05/28/2013, DOI 1.07507/1-4020-4494-1

BonTerra Consulting, 2010, Section 1605 Long-Term Streambed Alteration Agreement for the Debris Basin Maintenance Program, prepared for County of Los Angeles Department of Public Works on behalf of Los Angeles County Flood Control District, Web 12/20/2012, http://dpw.lacounty.gov/LACFCD/files/mnd.pdf.

Cannon, Susan H., 2001, Debris-flow generation from recently burned watersheds, Environmental and Engineering Geoscience, Nov 2001; 7: 321 - 341.

Cannon, S.H., Gartner, J.E., Rupert, M.G., Michael, J.A., Staley, D.M., and Worstell, B.B., 2010, Emergency assessment of postfire debris-flow hazards for the 2009 Station fire, San Gabriel Mountains, southern California: U.S. Geological Survey Open–File Report 2009-1227, 27 p. (Revised April 2010).

Cannon S.H., Gartner J.E., Rupert M.G., Michael J.A., Rea A.H., Parrett C., 2010, Predicting the probability and volume of post-wildfire debris flows in the intermountain western United States, Geological Society of America Bulletin 122(1-2), 127-144.

Cannon, Susan. H., Eric M. Boldt, Jayme L. Laber, Jason W. Kean, and Dennis M. Staley, 2011, Rainfall intensity-duration thresholds for post-fire debris-flow emergency response planning, Natural Hazards 59:209-236. Web 02/07/2013. DOI 1.07507/s11069-011-9747-2.

DiBiase RA, Whipple KX, Heimsath AM, Ouimet WB, 2010, Landscape form and millennial erosion rates in the San Gabriel Mountains, CA. Earth and Planetary Science Letters 289: 134–144, DOI 1.07516/j. epsl.2009.10.036.

Fire Effects on Soil, 2006, Factsheet 2, Fire Effects on Rangeland Factsheet Series, Web 03/30/2012, http://www.agf.gov.bc.ca/range/publications/documents/fire2.htm.

Gabet, Emmanuel J. and Paul Sternberg, 2008, The effects of vegetative ash on infiltration capacity, sediment transport, and the generation of progressively bulked debris flows, Geomorphology Volume 101, Issue 41 November, Pages 666-673, doi:1.07516/j.geomorph.2008.03.005.

Gatwood, Elden, John Pedersen, and Kerry Casey, 2000, Debris Method, The Los Angeles District Method for Prediction of Debris Yield, U.S. Army Corps of Engineers, Los Angeles District, Hydrology and Hydraulics Branch, Web 05/31/2013.

Hellmers, H., 1962, The San Gabriel Mountains--Man and Nature in Conflict, Engineering and Science, 25(8), 12-13.

Larsen, I. J., Montgomery, D. R. & Korup, O. 2010, Landslide erosion controlled by hillslope material. Nature Geosci. 3, 247–251, Web 06/12/2013.

Lavé J. and D. Burbank, 2004, Denudation processes and rates in the Transverse Ranges, southern California: erosional response of a transitional landscape to external and anthropogenic forcing, Journal of Geophysical Research 109: F01006. DOI. 1.07529/2003jf000023.

Loomis, J., P. Wohlgemuth, A. Gonzalez-Caban, and D. English, 2003, Economic benefits of reducing fire-related sediment in southwestern fire-prone ecosystem, Water Resources Res.39(9), 1260, doi:1.07529/2003WR002176.

Lourenço L., A. N. Nunes, A. Bento-Gonçalves and A. Vieira, 2012, Soil Erosion After Wildfires in Portugal: What Happens When Heavy Rainfall Events Occur?, Research on Soil Erosion, Dr. Danilo Godone (Ed.), ISBN: 978-953-51-0839-9, InTech, DOI: 10.5772/50447.

Lustig, Lawrence K., 1965, Sediment Yield of the Castaic Watershed, Western Los Angeles County California – A Quantitative Geomorphic Approach, Geological Survey Professional Paper 422-F, Web 06/26/2013, http://pubs.usgs.gov/pp/0422f/report.pdf.

Mathzone, 2013, Web 03/15/2013, http://www.emathzone.com/tutorials/geometry/area-of-a-segment.html.

Matti, J.C., Morton, D.M. and Cox, B.F., 1992, The San Andreas fault system in the vicinity of the central Transverse Ranges province, southern California: U.S. Geological Survey Open-File Report 92-354 , 40 p., scale 1:250,000, Web 03/29/2012.

McPhee, John, 1989, The Control of Nature, New York: Farrar, Straus, Giroux.

Moody, J.A., Smith, J.D., Ragan, B.W., 2005. Critical shear stress for erosion of cohesive soils subjected to temperatures typical of wildfires. Journal of Geophysical Research 110, F01004.

Notes on Measurement Errors, Web 03/15/2013, http://www.uoxray.uoregon.edu/phys290/ErrorNotes.pdf.

Nyman, Petter , Gary J. Sheridan, Hugh G. Smith, and Patrick N.J. Lane, 2011, Evidence of debris flow occurrence after wildfire in upland catchments of south-east Australia, Geomorphology, Volume 125, Issue 3, 1 February 2011, Pages 383-401.

Pak, Jang Hyuk and Joo Heon Lee, 2012, A Hyper-concentrated Sediment Yield Prediction Model Using Sediment Delivery Ratio for Large Watersheds, KSCE Journal of Civil Engineering 16(5):883-891, Web 05/29/2013, DOI 1.07507/s12205-012-1588-3.

Portenga, E. W. and R. R. Bierman. 2011, Understanding Earth's eroding surface with ^{10}Be, GSA Today. 21 (8): 4-10.

Radtke, K.W.H. (1983), Living More Safely in the Chaparral-Urban Interface, United States Department of Agriculture, Pacific Southwest Forest and Range Experimental Station.

Rulli, M. C., and R. Rosso, 2005, Modeling catchment erosion after wildfires in the San Gabriel Mountains of southern California, Geophys. Res. Lett., 32, L19401, doi:1.07529/2005GL023635.

Scott, KM and Williams RP, 1978, Erosion and Sediment Yields in the Transverse Ranges, Southern California, US Geological Survey Professional Paper 1030.

Sedimentation Manual, 2006, Los Angeles County Department of Public Works, Water Resources Division, Donald L. Wolfe, Director, 2nd Edition, Web 05/31/2013.

Sediment Management, 2013, Los Angeles County Department of Public Works, http://dpw.lacounty.gov/lacfcd/sediment/, Web 06/26/2013.

Shuriman G, and Slosson JE, 1992, Forensic engineering: environmental case histories for civil engineers and geologists, Chap 8, Academic Press, Harcourt Brace Javanovich, San Diego, pp 168–209.

Tan, S. S., 1998, Slope Failure and Erosion Assessment of the Fire Areas at Fillmore (April 1996) and Piru (August 1997), Ventura County, California: California Division of Mines and Geology Open File Report 98-32.

Tseng, Chih-Ming, Ching-Weei Lin, Colin P. Stark, Jin-Kin Liu, Li-Yuan Fei, Yu-Chung Hsieh, 2013, Application of a Multi-temporal, LiDAR-derived, Digital-Terrain Model in a Landslide-Volume Estimation, Earth Surface Processes and Landforms Revised Manuscript Draft, doi: 1.07502/esp.3454, Web 06/12/2013.

Warrick J.A., J.A. Hatten, G.B. Pasternack, A.B. Gray, M.A. Goni and R.A. Wheatcroft, 2012, The effects of wildfire on the sediment yield of a coastal California watershed, Geological Society of America Bulletin, DOI 10.1130/B30451.1.

Wells, W.G., 1987, The Effects of Fire on the Generation of Debris Flows in Southern California; in Costa, J.E. and Wieczorek, G.F. (editors), Debris Flows/Avalanches: Process, Recognition, and Mitigation: Geological Society of America Reviews in Engineering Geology, Vol. VII, pp. 105-114.

Yeats, R.S., 2004, Tectonics of the San Gabriel Basin and surroundings, southern California: Geological Society of America Bulletin, Vol. 116, pp. 1158-1182.

Appendix

Figure 1. Debris flow 2 (Gold Canyon)

a. Debris flow 2 - looking north up canyon

b. Debris flow 2 deposit - east, middle deposit

c. Debris flow 2 deposit - west, middle deposit

d. Debris flow 2 deposit - near the flow toe

Figure 2. Debris Flow 16 (Ybarra Canyon)

a. Debris flow 16 - looking up northeast

b. Debris flow 16 deposit - middle of flow deposit

c. Debris flow 16 - middle deposit, depth - 97 cm

d. Debris flow 16 deposit - near the flow toe

Figure 3. Debris Flow 22 (Pickens Canyon)

a. Active debris flow 22 view to north, mid-flow - taken by Carol Lewis from her La Canãda-Flintridge home on 02/16/10

b. Active debris flow 22 view to northeast, mid-flow - taken by Carol Lewis from her La Canãda-Flintridge home on 02/16/10

c. Active debris flow 22 view to northeast, mid-flow, closer view of deposits - taken by Carol Lewis from her La Canãda-Flintridge home on 02/16/10

d. Flow 22 deposit - west middle deposit

e. Debris flow 22 - looking south down flow deposits, field assistants: Joy Lee, Nathanael Ahlstrom, and Robert Dario from Morning Star Christian Academy

f. Debris flow 22 - looking down (south), bush to the left center is 2.3 m high

g. Debris flow 22 deposit - northwest view - center of deposit

h. Debris flow 22 deposit - northeast view - center of deposit

Figure 4. Debris flow 43 (Dark Canyon)

a. Debris flow 43 - looking north from Highway 2 - debris flow fence is 2.8 m high

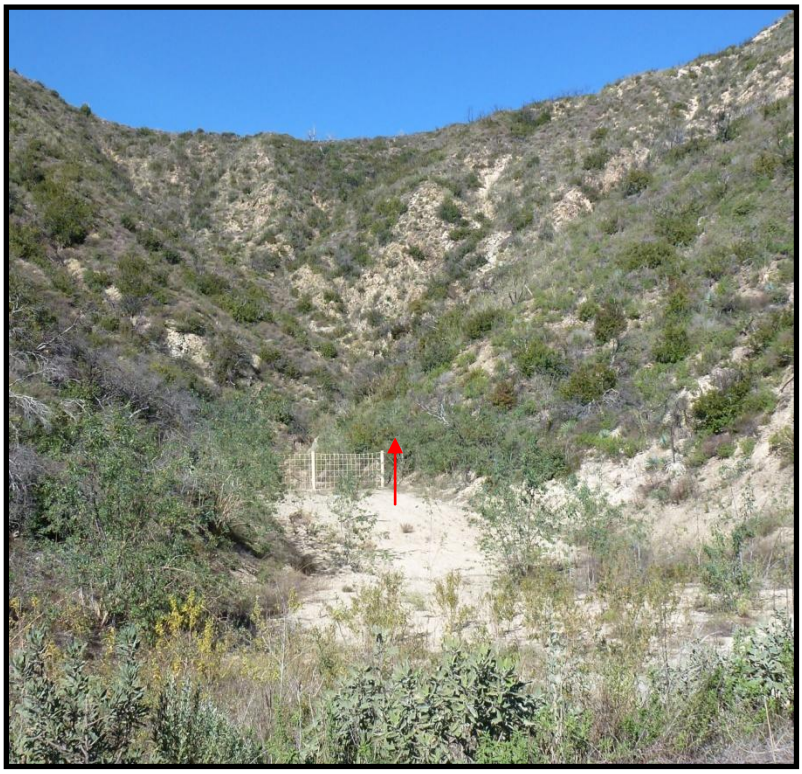

b. Debris flow 43 - west side of debris flow basin

c. Debris flow 43 - looking north up canyon, note east bush is 0.9 m high

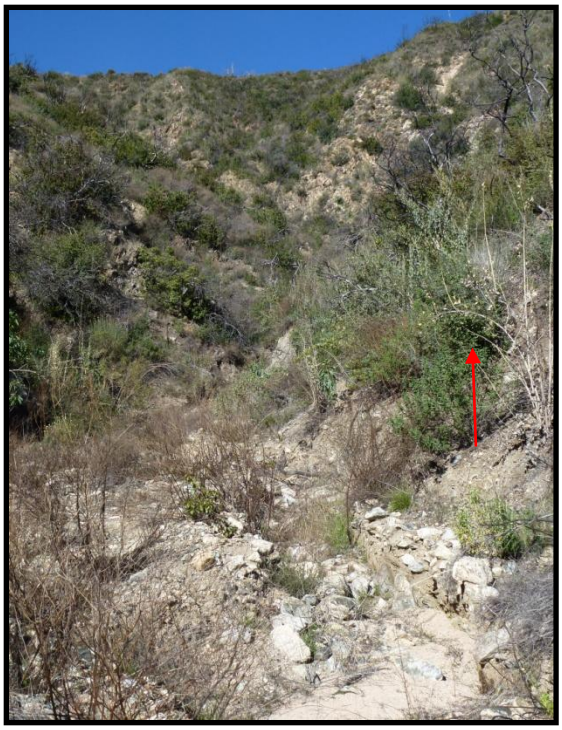

d. Debris flow 43 deposit- near the basin

Figure 5. Debris Flow 48 (proximal canyon to Delta Canyon)

a. Debris flow 48 - looking up north canyon from Big Tujunga Canyon Road - note burnt tree in center

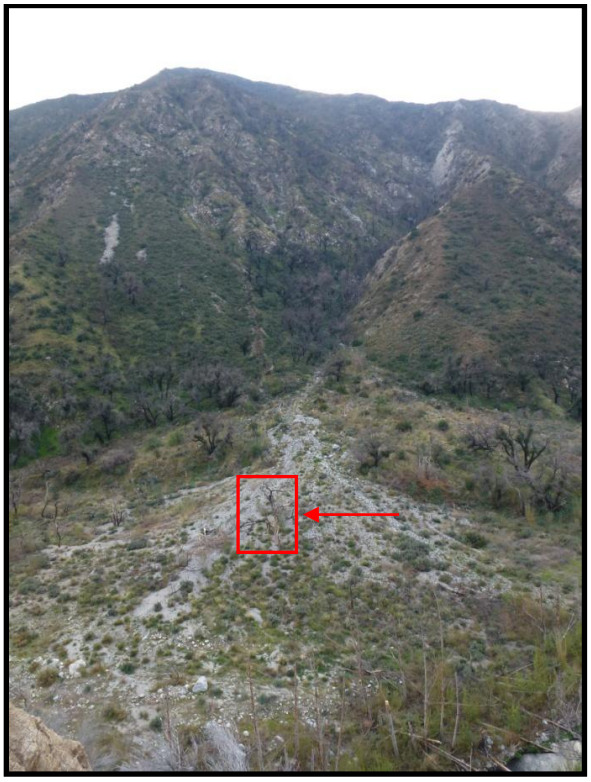

b. Debris flow 48 - looking up canyon from Big Tujunga Canyon Road (a closer view) - burnt tree is 3.4 m high

c. Debris flow 48 deposit - center of the deposit

d. Debris flow 48 debris - near the flow toe

Figure 6. Debris Flow 49 (Delta Canyon)

a. Debris flow 49 - looking south up canyon from Big Tujunga Canyon Road (outline is active debris flow) tree in middle of photo is 3.7 m high. Note the previous debris flow deposits on the left of the photo in yellow

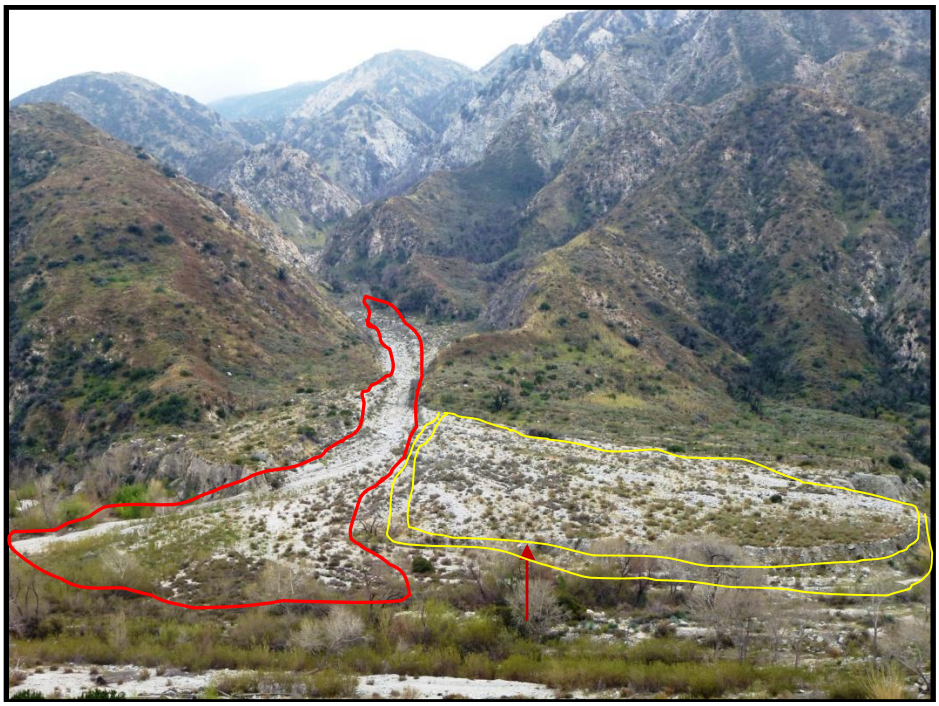

b. Debris flow 49 - looking south up from the east side, field assistants: Bryan Sanchez, Erica Rincon (CSUN Geological Sciences students), and Eric Ahlstrom

c. Debris flow 49 debris - looking south up canyon, mid-flow

d. Debris flow 49 - large boulder on east side of mid-flow

d. Debris 49 deposit on west canyon side wall

Figure 7. Debris Flow 50 (Vogel Canyon)

a. Debris flow 50 - Looking north from Big Tujunga Road - outline is flow deposit, note the debris gate (2.8 m high)

b. Debris flow 50 deposit - mid-flow

c. Debris flow 50 - looking north from mid-deposit, field assistant: Emelie Traub from LA Valley College

d. Debris flow 50 deposit on east - mid-flow deposit

Figure 8. Debris flow 52 (Stone Canyon)

a. Debris flow 52 - west middle deposit

b. Debris flow 52 - west side deposit, field assistant: Eric Ahlstrom

Figure 9. Debris flow 56 (Arroyo Seco Canyon)

a. Debris flow 56 deposit - west side, middle of the deposit

b. Debris flow 56 - looking south to debris flow basin, note tree (4 m high) in center of deposit

c. Debris flow 56 - looking further down south to debris flow basin - note telephone pole (3.7 m high) on the east side